16 Physiologically Based Pharmacokinetic (PBPK) Modeling: Usefulness and Applications

HAN-JOO MAENG[1,2], EDWIN C. Y. CHOW[1], JIANGHONG FAN[1], and K. SANDY PANG[1]

[1]University of Toronto, Toronto, Ontario, Canada
[2]Inje University, Gimhae, Gyeongnam, Korea

16.1 SUMMARY

Physiologically based pharmacokinetic (PBPK) models are increasingly being used to describe and define more meaningful parameters that relate to physiology, anatomy, and biochemistry in the prediction of pharmacokinetic (PK) profiles and tissue concentration–time profiles of the parent drug and metabolites and to provide mechanistic insight in drug dynamics. Physiological data (blood flow rates and tissue volumes), physical data (protein binding and tissue partition coefficients), and biochemical data (Michaelis–Menten parameters for transporters and enzymes, V_{max}/K_m) are the information required for building a PBPK model. Recently, single organ PBPK models for the intestine, liver, and kidney were applied to examine the influences of blood flow, protein binding, and activities of transporters and enzymes on the area under the curves (AUCs) and clearances of a drug and its formed metabolite. These in turn are used to build whole-body PBPK models consisting of the major drug elimination organs (i.e., intestine, liver, and kidney), together with

Encyclopedia of Drug Metabolism and Interactions, 6-Volume Set, First Edition.
Edited by Alexander V. Lyubimov.

highly perfused, poorly perfused, and adipose tissues. The whole-body PBPK model approach is extremely useful to understand sequential metabolism, the kinetics of metabolites, and examine effects of the transporter and enzyme interplay on the blood and target organ exposures of the drug and its metabolites. The application of PBPK models allows one to make predictions of the exposure in target sites, pharmacological activity, or toxicity and the effects of age, pregnancy, disease states, and drug–drug interactions (DDIs). In this chapter, cases for the application and usefulness of PBPK models are summarized.

16.2 INTRODUCTION

PK models represent mathematical descriptions that relate drug concentration levels to processes of drug absorption, distribution, metabolism, and excretion (ADME) *in vivo*. Various modeling approaches have been developed with varying degrees of complexity for applications in different situations. A popular approach is the classic PK compartmental modeling approach which describes the body as rapidly and/or poorly equilibrating compartments for the distribution of drugs/chemicals [1]. These models are the simplest and therefore the most widely used in the clinical setting to provide information on the extents of drug distribution and elimination. The major disadvantage of these models is that the plasma drug concentrations do not always reflect tissue drug concentrations that relate to drug responses and toxicological effects. Moreover, these approaches show serious limitations since the physiological processes, especially transporter function and the sequential handling of metabolites within metabolite formation organs, are not well described [2]. These limitations pave the way to the development of PBPK approaches.

PBPK models are increasingly being used to describe and define more meaningful parameters that relate to physiology, anatomy, and biochemistry. The approach is based on the assumption that compartments are homogeneous and well-stirred. The earliest description of PBPK models was introduced in the 1930s by Teorell, one of the pioneers of PK who applied mass balance equations on specific tissues and related to tissue volumes and organ perfusion rates on drug absorption, distribution, and elimination [3]. The elegant works of Bischoff and Dedrick during the 1950s–1970s then firmly established the importance of PBPK models in the prediction of drug protein binding, tissue distribution, and the disposition of thiopental and anticancer drugs in animals [4–6]. The usefulness of these models was evident, since animal data, when scaled up, were able to predict the concentration–time profiles in man [7,8]. The concepts are then used toward the description of eliminating organs [9–14].

The PBPK model consists of a number of subcompartments that represent actual tissues and organs of discrete volumes. The differential equations constructed for these models are based on three different classifications of parameters: physiological, thermodynamic/physical, and biochemical. Physiological parameters include tissue volumes (V) and tissue blood flow rates (Q) whose sum provides the cardiac output (Q_{CO}). One basic premise of PBPK models lies with the assumption that there is venous equilibration: the concentration in tissue blood equals that in the emergent blood. Thermodynamic parameters include protein binding (denoted as unbound fractions in plasma, blood, or tissue: f_P, f_B, or f_u, or f_T), the tissue to plasma/blood partition coefficient ($K_{P,T}$ or $K_{P,Tu}$) of the drug, and the transmembrane permeability. Biochemical

parameters exist as the result of metabolic and transport processes and are described by the constants, the V_{max} or maximum velocity and K_m, the Michaelis–Menten constant. The rate is given by the product of the substrate concentration [S] and the intrinsic clearance, CL_{int}. Under first-order conditions, the CL_{int} is given by V_{max}/K_m. The secretory intrinsic clearance ($CL_{int,sec}$) is responsible for renal, biliary, or luminal excretion. For transport, the influx (CL_{in}) and efflux (CL_{ef}) clearances are included to represent both the transporter-mediated and passive diffusion processes [15–18].

The prediction of PK profiles of new chemical entities in humans, based on *in vitro* and *in vivo* preclinical data, is an extremely useful technique that provides important information in the drug discovery and development phases to identify drug candidates with desirable, PK properties. These many useful features that appear in PBPK models are particularly pertinent in drug development [19–22] and health risk assessment [23–29]. Another feature rests on the scale-up of PBPK based on animal experiments (mouse, rat, dog, or monkey) to explain drug behaviors in humans [7,8,30–34]. Moreover, PBPK models have been routinely applied to predict tissue concentrations with respect to the route and dose of drug administration, and in the appraisal of how alteration of physiological or biochemical conditions such as in disease states [35–38] or genetic variants in transporters, enzymes, and/or protein binding would affect drug disposition [39,40].

Another area of development rests on single-organ PBPK models such as the intestine, liver, or kidney which furnish mathematical solutions comprising blood flow, protein binding, and transporter and enzymatic activity parameters for the AUC [15,16,18]. The relations among these parameters allow the examination of important determinants on organ clearances, the interplay between transporters and enzymes, and mechanisms of DDI within these frameworks [15,16,18]. These solutions pertain to the single organs and are readily used to compare the kinetics between formed and preformed metabolite.

In this chapter, we review the information needed for building a PBPK model and the general approaches used. We summarize the recently developed single-organ PBPK models for the intestine, liver, and kidney and whole-body PBPK models that are currently applied to gain a mechanistic understanding in drug disposition. The models can predict drug and metabolite concentrations in tissues at any time and provide mechanistic insight in drug dynamics. Currently, model predictions of lipophilic compounds surpass those which require transporter involvement for uptake and efflux or those that exhibit diffusion-limited transport. These PBPK models established for animals may be scaled up to man on the extrapolation of *in vitro* experimental findings to *in vivo* PK parameters.

16.3 BASIC CONSIDERATIONS

A general PBPK model is depicted in Fig. 16.1. The model consists of several tissue compartments that represent anatomic tissue regions in the body where the drug is distributed or metabolized/excreted. Enterohepatic circulation and renal reabsorption, processes that prolong the duration of drug and metabolite in the body, are readily incorporated. Although there is no general rule for the type of organ compartments to be included in the model, organs in which the drug exerts a pharmacologic and/or toxic response should be included. In principle, if all parameters that affect the disposition

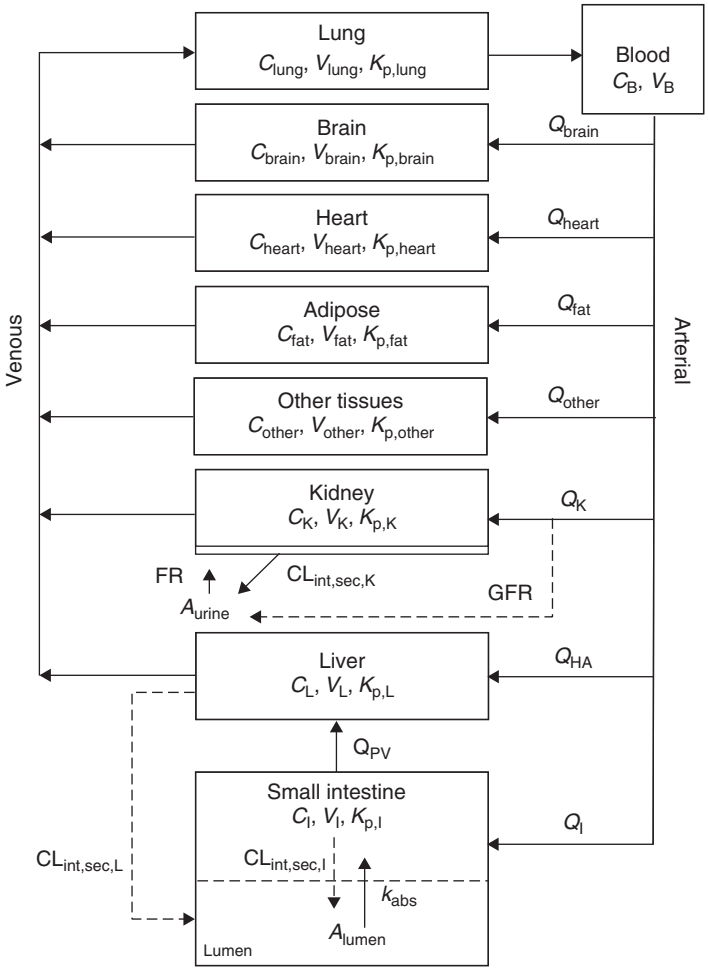

Figure 16.1 A physiologically based pharmacokinetic (PBPK) model of the whole body. Physiological volume (V), blood flow rate (Q), drug concentration (C), and tissue partition coefficient ($K_{P,T}$) in the brain ("$_{brain}$"), heart ("$_{heart}$"), lung ("$_{lung}$"), liver ("$_{L}$"), kidney ("$_{K}$"), intestine ("$_{I}$"), adipose tissue ("fat"), and other tissue ("$_{other}$") are some of the needed parameters for modeling; the blood is represented as ("$_{B}$"). FR is the fraction reabsorbed in the kidney, and GFR is the glomerular filtration rate.

of the drug are known *in vitro*, the model should be able to predict the PK of the drug *in vivo*. However, because of the complexities and differences inherent in the systems, many assumptions are needed to render a sound *in vitro*–*in vivo* extrapolation (IVIVE) before forming the proper mathematical relations to describe drug concentrations in the blood and tissues and physiological processes on transport, secretion, and metabolism within tissue compartments.

16.3.1 Physiological Data: Blood Flow Rates and Tissue Volumes

Blood flow rates and physiological tissue volumes are important parameters of PBPK models. Table 16.1 summarizes these flow parameters that show differences among

TABLE 16.1 Physiological Volumes and Blood Flow Rates in the Human, Rat, and Mouse[a]

Tissue	Human (70 kg)		Rat (0.25 kg)		Mouse (~0.02 kg)	
	Volume (mL)	Blood flow rate (mL/min)	Volume (mL)	Blood flow rate (mL/min)	Volume (mL)	Blood flow rate (mL/min)
Blood	5200	—	13.5	—	1.7	—
Brain capillary	1450	700	1.2	1.3	—	—
Brain capillary	—	—	—	—	0.025	0.089
Brain tissue	—	—	—	—	0.226	—
Heart	310	240	1.2	3.9	0.095	0.28
Kidney	280	1240	3.7	9.2	0.34	1.3
Liver	1690	—	19.6	—	1.3	—
Hepatic artery	—	300	—	2.0	—	0.35
Intestine	1650	1100	11.3	7.5	1.5	1.5
Lung	1170	—	2.1	—	0.1	—
Cardiac output (mL/min)	—	5600	—	14.0	—	8.0
GFR (mL/min)	—	125	—	1.31	—	0.28
Urine flow (mL/day)	—	1400	—	50.0	—	1.0

[a]from Refs 43 and 44

species. Blood flow is an important determinant in drug clearance in PBPK modeling. Although the pattern of blood flow, such as bulk flow, plug flow, or dispersive flow, into organs, such as the liver, affects the degree of mixing in the organ and transport and metabolic activities [10,41,42], bulk flow is usually considered. It is noteworthy that the blood flow rate to a specific organ may not reach the tissue site in its entirety. For example, part of the kidney plasma is filtered by glomerular filtration, and only the difference between the plasma flow and the GFR reaches the postglomerular tubular cells [11,12]. In the intestine, the blood flow reaching the enterocytes housing absorptive and secretory apical transporters and enzymes represents a small proportion of the entire intestinal blood flow [14].

16.3.2 Physical Data

16.3.2.1 Plasma Protein Binding. The binding of drugs to plasma protein usually retards the elimination of drugs. The pharmacological activity and toxicity of drugs are generally assumed to be correlated to the unbound drug concentration in the blood or tissue, and only the unbound drug is the species that is metabolized or excreted. Depending on whether the drug is a weak or strong acid or base, or is a neutral compound or zwitterion, it may bind to a single protein or multiple proteins (e.g., serum albumin, α_1-acid-glycoprotein, or lipoproteins) in blood [10,45]. For poorly extracted drugs, increasing the extent of binding to plasma proteins would decrease the rate of excretion in the kidney and the rate of metabolism in the liver [46,47], but binding exerts less influence on highly extracted drugs, whose elimination rates are more dependent on the blood flow [10,48]. Changes in plasma protein binding from disease states or DDIs may lead to clinical outcomes that require the adjustment of

dosage regimens. Therefore, drug binding to plasma proteins is a key determinant of clearance.

The binding of a drug to plasma proteins is usually a reversible process, denoted by the on (k_{on}) and off (k_{off}) rate constants. The ratio of these constants yields the binding association constant, K_A, and a value of less than 10^4/M suggests poor binding, whereas the one exceeding 10^4/M suggests tighter binding [49]. For the latter case, dramatic changes in the extent of protein binding are evoked on small changes in drug concentration when the binding association constant is high. The unbound plasma concentration, $C_{P,u}$, in plasma can be expressed as follows:

$$C_{P,u} = \frac{-(1 + nK_A P_t - K_A C_P) + \sqrt{(1 + nK_A P_t - K_A C_P)^2 + 4K_A C_P}}{2K_A} \tag{16.1}$$

where P_t is the protein concentration and n represents the number of binding sites within the same class of site. The bound plasma concentration ($C_{P,b}$) is expressed as the difference between the total (C_P) and unbound ($C_{P,u}$) plasma concentrations.

If the binding between a drug and plasma protein involves two classes of sites, one with low affinity and the other with higher affinity, such a binding involving two noncooperative affinities may be formulated as [50]

$$\frac{C_{P,b}}{C_{P,u}} = \frac{n_1 K_{A1} P_t}{1 + K_{A1} C_{p,u}} + \frac{n_2 K_{A2} P_t}{1 + K_{A2} C_{p,u}} \tag{16.2}$$

where K_{A1} and K_{A2} are the binding constants for class I and class II and n_1 and n_2 are the corresponding number of noncompetitive binding sites on the protein molecule. At low drug concentration, protein binding is not saturated and only the high affinity site is involved in the binding. When excess drug is present, the low affinity sites will be further recruited for binding. In such a case, the unbound fraction $C_{P,u}$ is a function of the binding to both the high and low affinity binding sites.

16.3.2.2 Tissue Partition Coefficient. The tissue partition coefficients are important drug-specific input parameters in PBPK modeling. The tissue–plasma (or plasma water) partition coefficient, $K_{P,T}$ (or $K_{P,Tu}$), is defined as the tissue (C_T) to the tissue plasma ($C_{T,P}$) (or plasma water ($C_{T,Pu}$) concentration ratio of the drug. Since the drug concentration in tissue plasma, total or unbound ($C_{T,P}$ or $C_{T,Pu}$), equals that leaving the tissue ($C_{T,P,out}$ or $C_{T,Pu,out}$), the following relations hold at steady state [9,51,52]:

$$K_{P,T} = \frac{C_{T,ss}}{C_{P,ss}} \text{ or } K_{P,Tu} = \frac{C_{T,ss}}{C_{Pu,ss}} \tag{16.3}$$

One may also express this ratio relative to the blood concentration.

The partition coefficient, when multiplied to the volume of the tissue, determines the effective volume of distribution of drug in the tissue ($V_{T,app}$). The sum of all the tissue volumes eventually provides the V_{ss}, or the steady-state volume of distribution, a commonly used parameter to denote the extent of drug distribution, as a plasma or blood equivalent volume [53].

There are several *in vitro* methods to determine $K_{P,T}$ within tissues, some of which are quite time consuming [54–56]. In addition, *in vivo* approaches exist for estimating

$K_{P,T}$ from blood and tissue after constant rate infusion or injection to animals [57–59]. These experimentally determined constants would underestimate the true $K_{P,T}$ (ratio of influx/efflux rate constants or influx/efflux intrinsic clearances) when elimination exists within the organ or tissue, since the denominator of Equation 16.3 is artificially increased due to the presence of the elimination rate constant or elimination intrinsic clearance [60].

Recent approaches have been developed for the prediction of $K_{P,T}$ [58,61,62]. These approaches require some understanding of the physiochemical properties of the drug as well as distribution mechanisms or binding to tissue neutral lipids, phospholipids, and intracellular water. However, most of the models are suitable for small neutral molecules only and will result in significant inaccuracies when applied to compounds that are extensively ionized at physiological pH. To solve this problem, Rodgers and Rowland [63] incorporated drug ionization in both intra- and extracellular water into the approaches developed by Poulin *et al*. [62]. Under physiological condition, basic drugs ($pK_a \geq 7$) such as β-blockers are sufficiently ionized; their electrostatic interaction with acidic phospholipids predominates and accounts for the tissue binding (Eq. 16.4) [63,64]. For acids, very weak bases, neutrals, and zwitterions, their binding to extracellular proteins contributes to the binding and the electrostatic force towards acidic phospholipids is minimal (Eq. 16.5) [63,65].

For basic compounds, K_{pu} is

$$K_{pu} = \left[\left(\frac{1 + X \cdot f_{IW}}{1 + Y}\right) + f_{EW} + \left(\frac{K_{A,AP}[AP]_T \cdot X}{1 + Y}\right) + \left(\frac{P \cdot f_{NL} + (0.3P + 0.7) f_{NP}}{1 + Y}\right)\right] \tag{16.4}$$

For acids, very weak bases, neutrals, and zwitterions, K_{pu} is

$$K_{pu} = \left[\left(\frac{1 + X \cdot f_{IW}}{1 + Y}\right) + f_{EW} + (K_{A,PR}[PR]_T) + \left(\frac{P \cdot f_{NL} + (0.3P + 0.7) f_{NP}}{1 + Y}\right)\right] \tag{16.5}$$

where P is the octanol:water partition coefficient or concentration ratio of the unionized compound in all tissues except the adipose tissue, whose partition coefficient is assessed as the vegetable or olive oil:water partition coefficient or concentration ratio; f is the fractional tissue volume; subscripts IW and EW represent the intracellular and extracellular tissue water, respectively; NP and NL denote the neutral phospholipids and neutral lipids, respectively; $[AP]_T$ is the tissue concentration of acidic phospholipids; and $[PR]_T$ is concentration of extracellular albumin (for acid and weak base) or lipoprotein (for neutral compounds). The terms, X, Y, and Z, are terms that account for the extents of drug ionization as defined in Table 16.2.

$K_{A,AP}$ in Equation 16.4 is the binding association constant for the interaction between basic drugs to acidic phospholipids, and $K_{A,PR}$ in Equation 16.5 is the binding association constant for the interaction between acidic or neutral compounds, weak bases, or zwitterions and extracellular albumin/lipoprotein. For weak bases, the binding association constant in red blood cells (RBCs), $K_{A,RBC}$, may be estimated using

TABLE 16.2 Definition of the Terms X, Y, and Z in Equations 16.4–16.8

	X	Y	Z
Monoprotic base	$10^{pK_a - pH_{IW}}$	$10^{pK_a - pH_P}$	$10^{pK_a - pH_{BC}}$
Diprotic base[a]	$10^{pK_{a2} - pH_{IW}} + 10^{pK_{a1} + pK_{a2} - 2pH_{IW}}$	$10^{pK_{a2} - pH_p} + 10^{pK_{a1} + pK_{a2} - 2pH_p}$	$10^{pK_{a2} - pH_{BC}} + 10^{pK_{a1} + pK_{a2} - 2pH_{BC}}$
Monoprotic acid	$10^{pH_{IW} - pK_a}$	$10^{pH_P - pK_a}$	NA
Diprotic acid[a]	$10^{pH_{IW} - pK_{a1}} + 10^{2pH_{IW} - pK_{a1} - pK_{a2}}$	$10^{pH_P - pK_{a1}} + 10^{2pH_P - pK_{a1} - pK_{a2}}$	NA
Zwitterion	$10^{pK_{a,BASE} - pH_{IW}} + 10^{pH_{IW} - pK_{a,ACID}}$	$10^{pK_{a,BASE} - pH_P} + 10^{pH_P - pK_{a,ACID}}$	$10^{pK_{a,BASE} - pH_{BC}} + 10^{pH_{BC} - pK_{a,ACID}}$
Neutral	0	0	NA

[a]In these expressions $pK_{a1} < pK_{a2}$; pHp is the pH of plasma
Abbreviation: NA, not available.

Equation 16.6 with the known unbound fractions ($f_{IW,RBC}$, $f_{NL,RBC}$, and $f_{NP,RBC}$), the X, Y, and Z terms from Table 16.2, and $K_{Pu,RBC}$ from Equation 16.7; the $K_{A,RBC}$ so estimated is assumed to equal $K_{A,AP}$, which, in turn, may be applied to estimate K_{pu} in Equation 16.4:

$$K_{A,RBC} = \left[K_{Pu,RBC} - \left(\frac{1+Z}{1+Y} f_{IW,RBC}\right) - \left(\frac{P \cdot f_{NL,RBC} + (0.3P + 0.7) f_{NP,RBC}}{1+Y}\right)\right] \left(\frac{1+Y}{Z[AP]_{RBC}}\right) \tag{16.6}$$

$$K_{Pu,RBC} = \frac{\text{Hct} - 1 + \left(\frac{C_B}{C_P}\right)}{f_P \text{Hct}} \tag{16.7}$$

Specifically, $K_{Pu,RBC}$ is the ratio of drug concentration in RBCs to that unbound in plasma and represents the binding association constant of drug molecules to RBCs. C_B/C_P is the blood:plasma concentration ratio and Hct is the hematocrit; f_P is the fraction of drug unbound in plasma; and subscripts RBC and P denote the red blood cells and plasma, respectively.

For acidic, neutral, and weakly basic compounds or zwitterions, the binding association constant $K_{A,PR}$ is given by the following equation:

$$K_{A,PR} = \left[\frac{1}{f_P} - 1 - \left(\frac{P f_{NL,P} + (0.3P + 0.7) f_{NP,P}}{1+Y}\right)\right] \left(\frac{1}{[PR]_P}\right) \tag{16.8}$$

After obtaining the K_{Pu} values, the V_{ss} is calculated as

$$V_{ss} = V_P + f_P \sum V_{T,i} K_{Pu,T,i} \tag{16.9}$$

where V_P is the volume of plasma and $V_{T,i}$ is the volume of the ith tissue/organ; the term $V_{T,i} K_{Pu,T,i}$ is $V_{T,app}$ or the apparent volume of the tissue compartment for the ith tissue/organ [63]. Equation 16.9 is a general approach to estimate the steady-state volume of distribution, V_{ss}.

However, PBPK models are very complex and the number of organ/tissue compartments can exceed 15 or more [19,66]. A strategy for simplification is to lump the compartments and reduce the complexity of the PBPK model without loosing the predictive power. The underlying strategies are as follows: (i) tissues with same model specification for flow or partition (e.g., both are highly/poorly perfused or of similar K_p) and of same position in the system structure can be lumped together; (ii) serial tissues that equilibrate with one another rapidly should be lumped; and (iii) parallel tissues that have similar rate constants may be lumped [19]. It was suggested that the preliminary estimation of V_{ss} can be based solely on $K_{P,muscle}$ and $K_{P,fat}$ [59,61,63] since drug distribution into muscle and fat accounts for approximately 65–84% of the total V_{ss}; the $K_{P,muscle}$ may be used for all lean tissues except for the lungs which are represented by the $K_{P,fat}$ [59]. This new idea provides a time-efficient prediction of $K_{P,T}$ for lumped compartments in developing the PBPK models.

16.3.3 Biochemical Data on Enzymes and Transporters

The basic tissue compartment usually represents an individual organ or a group of "lumped" organs/tissues with similar flow parameter or partition characteristics. After giving consideration to the above general concepts, there is the need to consider transporters and enzymes (see Chapters 5–7) as important biochemical parameters in building a PBPK model. Rate equations may then be used to describe the transport and enzymatic processes. For the description of rate processes, the simplest Michaelis–Menten equation is often used, wherein the rate, v, is expressed in terms of the intrinsic clearance for transport, metabolism, and/or secretion (CL_{in}, CL_{ef}, $CL_{int,met}$, or $CL_{int,sec}$):

$$v = \frac{V_{max}}{K_m + [S]}[S] = CL_{int}[S] \tag{16.10}$$

The intrinsic clearance for a particular process is the maximum velocity, V_{max}, divided by the sum of the Michaelis–Menten constant, K_m, and the unbound substrate concentration, [S] or $V_{max}/(K_m + [S])$. For this reason, the binding of the drug to microsomes/cytosol must be examined to better define [S] [67–69]. The V_{max} and K_m values are usually obtained from *in vitro* studies, commonly estimated from the rate plot (v vs [S]), the Lineweaver–Burk, Eadie–Hofstee, or Hanes–Woolf plot. Usually, the assumption is that elimination is first order, and CL_{int} is the ratio of V_{max}/K_m. The *in vitro* intrinsic metabolic clearance under linear conditions is given by [70]

$$CL_{int,met,in\,vitro} = \frac{V_{max}}{K_m} \tag{16.11}$$

Metabolic or enzyme functions, estimated from human liver microsomal and cytosolic incubations, supersomes or recombinant expression systems, and the appropriate scaling factors, are converted to per gram liver when the hepatocellularity (cells per gram liver), microsomal protein (mg/g liver), and the overall expression of the cytochrome P450 (CYP) enzyme (pmol/g liver) are involved in converting the *in vitro* data to provide the $CL_{int,met}$ in human liver *in vivo* [43,71–73]. Preference of recombinant systems over human liver microsomes (HLMs) has been expressed, offering improved assay sensitivity compared with HLM for $CL_{int,met}$ determination [74].

The transporter-mediated processes and passive diffusion into and out of the tissue compartment must be summed to yield the influx (CL_{in}) and efflux (CL_{ef}) clearances, respectively. Normally, transporter function may be estimated in cell expression systems, combined with human transporter uptake studies. The influx transport intrinsic clearance (CL_{in}) is usually estimated from *in vitro* hepatic uptake studies. However, quantitative data on how much protein of each of the transporters is expressed within different tissue region is lacking to accurately define the relative proportions or abundancy of sinusoidal transporters for uptake and apical transporters for excretion. Moreover, the localization of the transporter, whether within the cytosol or nucleus or on the membrane surface would greatly affect the transport rate. In order to gain this insight, use of proteomics, with LC-MS/MS technologies to provide the absolute quantification of transporters, must be completed to provide the relative proportions of transporters in the liver, kidney, and blood–brain barrier [75,76]. In absence of these data, hepatocyte uptake information for extrapolation of *in vitro* parameters to *in vivo*,

cell number per unit tissue weight and tissue weight per unit body weight, in addition to the physiological scaling factors, have been used [39,77–79]. At a qualitative level, *in vitro* uptake and biliary excretion data using the rat and human sandwich-cultured hepatocyte systems may be used to assess whether there is species similarity and correlation to the *in vivo* plasma and biliary clearances [80] or DDI in transport; care must be included to describe differences in transporter expression in the system as well as real species differences. Indeed, *in vitro* data have identified marked species differences for the MRPs (multidrug resistance-associated proteins) and BCRP (breast cancer resistance protein) in rat and human hepatocytes; these significant species differences in efflux transporter activities could be integrated into animal data for the prediction of human transport [81]. When there is no significant interspecies difference between rat and man, the scaling factor determined in rats has been used to extrapolate human *in vitro* parameters to those *in vivo*. The transporter-mediated transport clearance should then be considered, in addition to the passive clearance, for the prediction of *in vivo* intrinsic influx and efflux clearances.

16.4 TYPES OF MODELS

Two tissue type models are considered: the membrane-limited model and blood flow-limited model (Fig. 16.2a and b). These PBPK models are also extended to describe the sequential metabolism or the excretion of formed metabolites (Fig. 16.2c). In any one PBPK model, a mixture of these may be used. The membrane-limited subcompartment is used for poorly permeable tissues, whereas for other tissue sites that rapidly equilibrate with blood, the flow-limited compartment may be used.

16.4.1 Membrane-Limited Model

Each tissue compartment basically consists of three well-mixed subcompartments: a vascular space that houses the blood that is perfusing the tissue, an interstitial space, and a cellular space (Fig. 16.2a). The drug enters with the afferent tissue blood flow (Q_T) with arterial concentration (C_A) into the vascular subcompartment, where there is instantaneous equilibrium with drug in the interstitium (C_{TI}). For all intents and purposes, the interstitial space may be combined with the vascular space to yield the extracellular compartment representing the tissue blood subcompartment of concentration, C_{TB}. With venous equilibration, C_{TB} equals the efferent blood concentration ($C_{T,out}$). The rate equations and the clearance terms used to describe the transport and enzymatic processes are the intrinsic clearances (CL_{in} and CL_{ef}) for influx and efflux at the basolateral membrane, respectively, and $CL_{int,sec}$ and $CL_{int,met}$ for excretion at the apical membrane and metabolism within the tissue.

Within the tissue compartment, the drug may become bound to tissue proteins, metabolized by enzymes with metabolic intrinsic clearance, $CL_{int,met}$, or is effluxed out of the cell by transporters and/or passive diffusion (CL_{ef}), or excreted at the apical membrane ($CL_{int,sec}$). The rate equations for the tissue blood (TB) and tissue (T) compartments are

$$V_{TB}\frac{dC_{TB}}{dt} = Q_T C_A - Q_T C_{T,out} + f_T C_T CL_{ef} - f_B C_{TB} CL_{in} \tag{16.12}$$

$$V_T\frac{dC_T}{dt} = f_B C_{TB} CL_{in} - f_T C_T (CL_{ef} + CL_{int}) \tag{16.13}$$

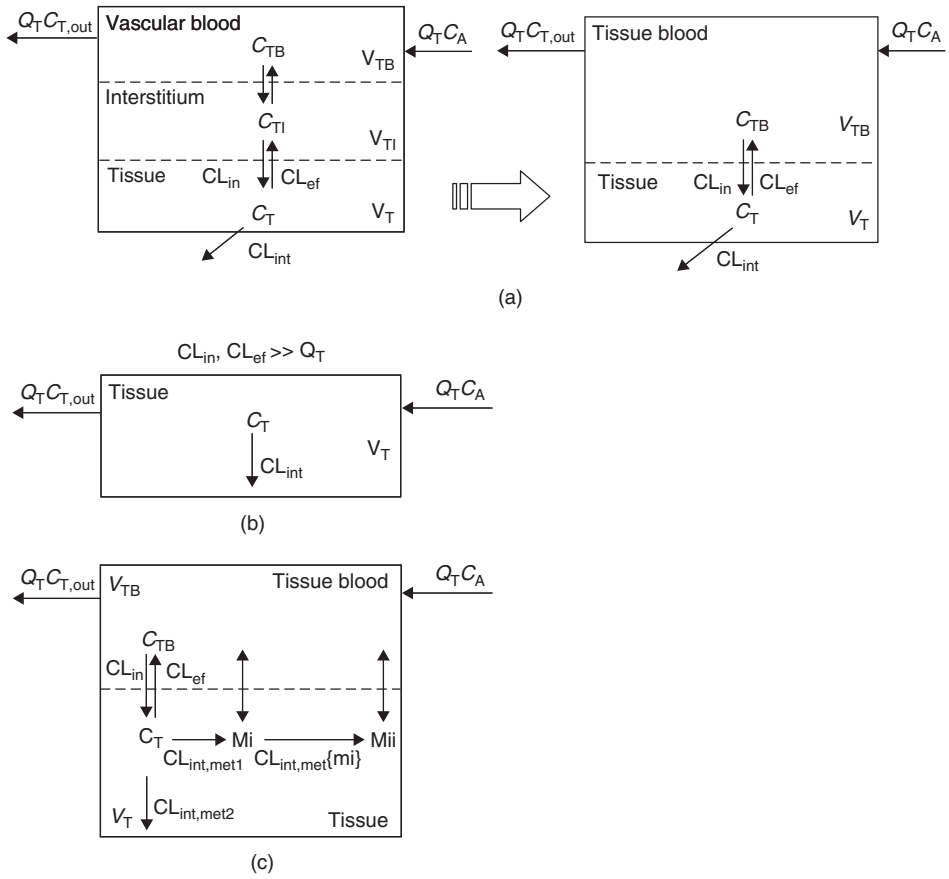

Figure 16.2 Typical PBPK components within an organ. There are two types of tissue models: (a) membrane limited; (b) blood flow limited; and (c) sequential metabolism of the formed primary metabolite (Mi) from parent drug (P) to the secondary metabolite (Mii) may occur within the organ of formation.

where f_B and f_T are the unbound fractions in blood and tissue, respectively, and CL_{int} is the total intrinsic clearance (sum of $CL_{int,met}$ and $CL_{int,sec}$).

16.4.2 Flow-Limited Model

The above relations are simplified with the assumption that the transfer across the membrane is rapid compared to the perfusion rate of the tissue (CL_{in} and $CL_{ef} \gg Q_T$). This means that the vascular, interstitial, and cellular subcompartments are in rapid equilibrium. As a result, these three subcompartments are combined to form one tissue compartment (Fig. 16.2b). The tissue to blood/plasma concentration ratio ($K_{P,T}$ or $C_T/C_{T,out}$) is used in this simplification. The mass balance equation can be written as

$$V_T\frac{dC_T}{dt} = Q_TC_A - Q_TC_{T,out} - f_TC_TCL_{int} = Q_TC_A - Q_T\frac{C_T}{K_{p,T}} - f_TC_TCL_{int} \quad (16.14)$$

where $C_T/K_{P,T}$ replaces $C_{T,out}$.

16.4.3 Model for Sequential Metabolism

The membrane-limited and flow-limited PBPK models are readily extended to describe the formation and sequential handling of the metabolite [82]. The PBPK model serves to describe sequential metabolism very well [15,82], especially when the nascently formed metabolite is immediately metabolized or excreted [83–85]. The rate equations for the tissue blood (TB) and tissue (T) compartments are expressed in Equations 16.15 and 16.16. Note that the set of parameters pertaining to the metabolite are qualified by {mi} for the concentrations, the binding constants, and the transport intrinsic clearances:

$$V_{TB}\frac{dC_{TB}\{mi\}}{dt} = Q_T C_A\{mi\} - Q_T C_{T,out}\{mi\} + f_T\{mi\}C_T\{mi\}CL_{ef}\{mi\} - f_B\{mi\}C_{TB}\{mi\}CL_{in}\{mi\} \quad (16.15)$$

Within the metabolite formation organ, the metabolite is immediately removed by intrinsic clearance, $CL_{int,met}\{mi\}$, and PBPK modeling considers the sequential handling of the formed metabolite [2]:

$$V_T\frac{dC_T\{mi\}}{dt} = f_T C_T CL_{int,met} + f_B\{mi\}C_{TB}\{mi\}CL_{in}\{mi\} - f_T C_T\{mi\}(CL_{ef}\{mi\} + CL_{int,met}\{mi\}) \quad (16.16)$$

PBPK metabolite modeling allows one to compare the kinetics between the formed versus preformed metabolite and brings a new perspective to differences in the kinetics of formed versus preformed metabolite. This is an interesting aspect for safety considerations of metabolites, if the information on the kinetics of the formed metabolite is predicted/gained on administration of a preformed metabolite, as in metabolite-in-safety testing (MIST) [15,86]. Use of the PBPK model will provide more accurate predictions on the kinetics of sequential metabolism for the investigation of risk assessment and toxicity associated with drug metabolite. However, there is a divergence for metabolite handling when metabolites display poor permeability across biological membranes [83,87,88]. The membrane barrier bars the metabolite from entering or leaving the tissue, thereby rendering differences in fates of the formed versus preformed metabolite kinetics.

16.5 PBPK MODELS OF ORGANS

The development of PBPK models, especially on simple organs for drugs and metabolites, has provided solutions for the AUCs and clearances for a drug and its formed metabolite. Rate equations are written for each subcompartment, providing the essential coefficients for matrix inversion and solutions which yield the steady-state concentrations/AUCs of the drug and of the metabolite (AUC{mi, P}) [15]. The method of matrix inversion, appropriate only under linear kinetic conditions, has been applied to examine whether AUC{mi, P} is suitable for estimation of the systemic bioavailability [18].

16.5.1 The Liver

A liver PBPK model that describes membrane-limited transport, with either fast or slow transmembrane transport clearances for summed diffusion-limited and transporter-mediated transport cases, denoted as CL_{in} and CL_{ef}, has been developed [89,90]. The model comprises of four compartments: the reservoir (R, or blood compartment), liver blood (LB), liver tissue (L), and bile compartment (bile) (Fig. 16.3) [15]. The hepatic flow rate and unbound fraction in blood and liver are denoted by Q_H, f_B, and f_L, respectively. The transport processes underlying carrier-mediation and passive diffusion are denoted by the influx and efflux intrinsic clearances (CL_{in}^H and CL_{ef}^H) representing the summed activities of basolateral transporters and passive diffusion (Fig. 16.3). In addition, biliary secretion at the apical membrane and metabolism within hepatocytes are denoted by the biliary intrinsic clearance ($CL_{int,sec,H}$) and metabolic intrinsic clearance ($CL_{int,met,H}$) of phase I and phase II enzymes, respectively (Fig. 16.3). The model also serves to describe hepatic sequential metabolism [2,15,82,84], in which the metabolite formed within the liver tissue is prone to sequential metabolism immediately to form other metabolites ($CL_{int,met,H}\{mi\}$) or is immediately excreted ($CL_{int,sec,H}\{mi\}$).

An advantage of PBPK model is that solutions relating to blood flow, protein binding, and activities of the transporters and enzymes for the elimination of the drug and metabolite may be derived by matrix inversion from the rate equations for the drug and metabolite [15,18,91]. Pang *et al*. [15] had summarized the AUC from time 0 to ∞ for the drug and the metabolite for the liver PBPK model. As shown in Table 16.3, the AUC of the drug is a complex equation that relates to the flow rate (Q_H), f_B, CL_{in}^H, and CL_{ef}^H, and the total hepatic intrinsic clearance ($CL_{int,H}$). In the case of a drug of

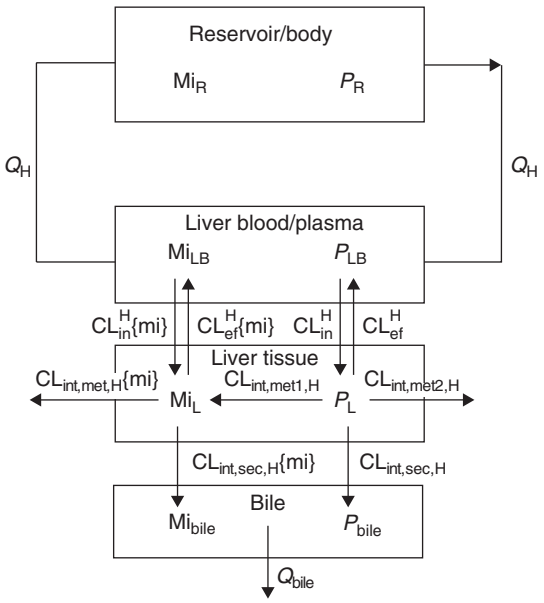

Figure 16.3 Physiologically based pharmacokinetic (PBPK) liver model, with liver as the only elimination organ. See text for description of the model.

flow-limited distribution (i.e., when $CL_{in}^{H} \cong CL_{ef}^{H} > Q_H$), these equations are simplified (Table 16.3). The ratio of hepatic metabolic and biliary clearances, $CL_{H,met}/CL_{H,sec}$ equals the ratio of the intrinsic clearances, $CL_{int,met,H}/CL_{int,sec,H}$. From this relation, the unknown parameter, $CL_{int,sec}$ may be obtained with the data from liver perfusion studies or *in vivo* studies [92] when $CL_{int,met}$ is obtained from *in vitro* metabolism studies using 9000*g* supernatant fractions or liver microsomes. These equations shown in Table 16.3 are useful to allow inferences on mechanisms of DDIs in the liver to be made.

The AUC for the formed metabolite, $AUC_{iv}\{mi,P\}$, after iv dosing of the precursor drug is dependent on the formation (metabolic) intrinsic clearance from the drug, $CL_{int,met1,H}$, and individual components of the $CL_{int,H}$ (or $CL_{int,met1,H} + CL_{int,met2,H} + CL_{int,sec,H}$), as well as binding, transport clearances ($CL_{in}^{H}\{mi\}$ and $CL_{ef}^{H}\{mi\}$), and intrinsic clearance, $CL_{int,H}\{mi\}$, of the metabolite [sum of ($CL_{int,met,H}\{mi\}$) and ($CL_{int,sec,H}\{mi\}$)]. In contrast, the AUC obtained from administration of its preformed counterpart that yielded $AUC_{po}\{pmi\}$ and $AUC_{iv}\{pmi\}$ is independent of drug parameters [15,86]. Indeed, solutions for the formed metabolite after oral and intravenous drug dosing ($AUC_{po}\{mi,P\}$ and $AUC_{iv}\{mi,P\}$) have revealed interesting differences from $AUC_{po}\{pmi\}$ and $AUC_{iv}\{pmi\}$ that result from the administration of the preformed counterpart [15,86].

Other aspects that contribute to differences between $AUC_{po}\{mi,P\}$ and $AUC_{iv}\{mi,P\}$ after drug dosing and $AUC_{po}\{pmi\}$ and $AUC_{iv}\{pmi\}$ after preformed metabolite dosing have been attributed to the heterogeneity of transporters and metabolic enzymes. As an improvement, zonal PBPK liver models consisting of three zonal regions: zones 1 (periportal zones), 2 (midzonal zones), and 3 (perivenous zones) or models similar to compartments in series have been developed [92–95]. Another factor is the presence of a basolateral membrane barrier for the metabolite, retarding entry or efflux of preformed metabolite into and out of cells but trapping the formed metabolite within the tissue [83,87,88,96]. Many successful examples of zonal PBPK modeling include enalapril [89,94], morphine [97], estrone sulfate [98], estradiol−17β-glucuronide [99], and digoxin [95], which were all investigated within rat liver perfusion studies. Furthermore, the role of the efflux transporter, Mrp2, which is responsible for excretion of both the parent drug, estradiol−17β-glucuronide and its 3-sulfate−17β-glucuronide metabolite on net desulfation, was elucidated comprehensively within the framework of a liver PBPK model [99,100].

Digoxin, a cardiotonic agent, is an example of a poorly cleared compound whose uptake into hepatocytes is rapid due to passive diffusion and the transporter, Oatp1a4, and whose clearance may be rate-limited by binding to RBCs and albumin [95]. Moreover, for poorly cleared substrates, heterogeneity in the metabolic activities among zones fails to affect the overall clearance when the drug concentration gradient within the sinusoid is shallow [92]. Drugs that are highly extracted exhibit a steep concentration gradient in the sinusoid, and, under this instance, removal rates are greatly modulated by enzyme/transporter heterogeneity. Sequential metabolism in liver could be affected by the zonal localization of metabolic enzymes. For example, different metabolites were observed for salicylamide versus gentisamide, hydroxylated metabolite of salicylamide, administration: due to the close proximity of hydroxylation and glucuronidation enzymes in the sequential metabolism of salicylamide, gentisamide glucuronidation predominates over sulfation; in contrast, gentisamide sulfate conjugates are more abundant when gentisamide is administered [85,101,102].

TABLE 16.3 Equations on the Area Under the Curve (AUC) and Total Hepatic Clearance ($CL_{H,\,tot}$)

Parameters	Membrane-Limited Case	Flow-Limited Case
AUC_{iv}	$\frac{\text{Dose}_{iv}\left[Q_H\left(CL_{ef}^H + CL_{int,H}\right) + f_B CL_{in}^H CL_{int,H}\right]}{f_B CL_{in}^H Q_H CL_{int,H}}$	$\frac{\text{Dose}_{iv}\left[\left(Q_H + f_B CL_{int,\,H}\right)\right]}{Q_H f_B CL_{int,\,H}}$
$AUC_{iv}\{mi,P\}$	$\frac{\text{Dose}_{iv} CL_{int,met1,H} CL_{ef}^H\{mi\}}{\left(CL_{int,met1,H}+CL_{int,met2,H}+CL_{int,sec,H}\right) f_B\{mi\} CL_{in}^H\{mi\} CL_{int,H}\{mi\}}$	$\frac{\text{Dose}_{iv} CL_{int,\,met1,\,H}}{\left(CL_{int,\,met1,\,H}+CL_{int,\,met2,\,H}+CL_{int,\,sec,\,H}\right) f_B\{mi\} CL_{int,\,H}\{mi\}}$
$CL_{H,\,tot}$ (total hepatic clearance)	$Q_H \frac{f_B CL_{int,H} CL_{in}^H}{Q_H CL_{ef}^H + CL_{int,H}\left(Q_H + f_B CL_{in}^H\right)}$	$\frac{Q_H f_B CL_{int,\,H}}{\left[\left(Q_H + f_B CL_{int,\,H}\right)\right]}$
$CL_{H,\,met1}$ (formation clearance of Mi)	$Q_H \frac{f_B CL_{int,met1,H} CL_{in}^H}{Q_H CL_{ef}^H + CL_{int,H}\left(Q_H + f_B CL_{in}^H\right)}$	$\frac{Q_H f_B CL_{int,\,met1,\,H}}{\left[\left(Q_H + f_B CL_{int,\,H}\right)\right]}$
$CL_{H,\,met2}$ (metabolic clearance for formation of other metabolites)	$Q_H \frac{f_B CL_{int,met2,H} CL_{in}^H}{Q_H CL_{ef}^H + CL_{int,H}\left(Q_H + f_B CL_{in}^H\right)}$	$\frac{Q_H f_B CL_{int,\,met2,\,H}}{\left[\left(Q_H + f_B CL_{int,\,H}\right)\right]}$
$CL_{H,\,ex}$ (biliary clearance of drug)	$Q_H \frac{f_B CL_{int,sec,H} CL_{in}^H}{Q_H CL_{ef}^H + CL_{int,H}\left(Q_H + f_B CL_{in}^H\right)}$	$\frac{Q_H f_B CL_{int,\,sec,\,H}}{\left[\left(Q_H + f_B CL_{int,\,H}\right)\right]}$

Source: From Sun and Pang [18] with permission.

16.5.2 The Small Intestine: Traditional Model (TM) and Segregated Flow Model (SFM)

Drugs administered orally are first absorbed, either passively or via active/facilitated transport, across the intestinal luminal membrane to reach the systemic circulation. The various intestinal transport proteins present on the apical membrane are known to participate in the uptake of drugs. Efflux by adenosine triphosphate (ATP)-binding cassette transporters delimits drug absorption in the intestine, whereas absorptive transporters mediate drug absorption [103–105]. Additionally, the intestine possesses the conjugating enzymes, UDP-glucuronosyl transferases) and GST (glutathione S-transferases) [106,107], and CYP3A, accounting for ~80% of the total immunoquantified CYPs [108–112] that play important roles in reducing oral bioavailability. Processes of intestinal absorption, metabolism, and secretion must be considered simultaneously in viewing oral drug bioavailability, and PBPK models have been developed to describe these processes [14,104,113,114].

A traditional, physiologically based model (traditional model, TM), which regards the intestine as a single homogeneous compartment with all of the intestinal blood flow perfusing the tissue, has been developed to account for oral drug bioavailability (Fig. 16.4a) [13]. This model encompasses all the variables of transport, metabolism, efflux, gastrointestinal transit, and absorption. In this model, the intestine is composed of three subcompartments: intestinal blood, tissue, and lumen. The blood or reservoir (R or blood compartment) of volume V_R and intestine compartments are interconnected

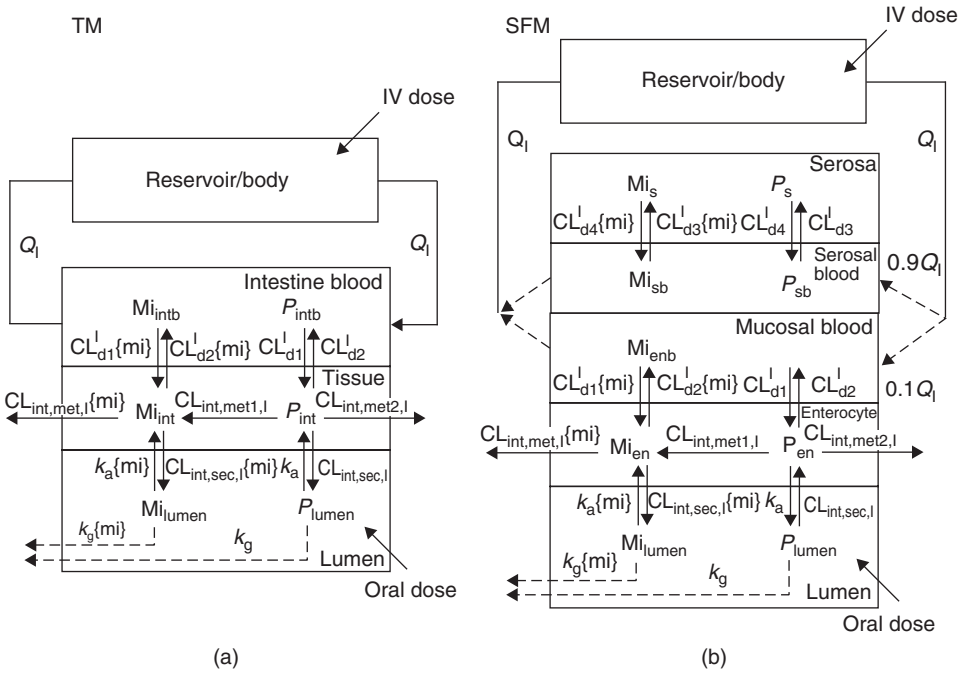

Figure 16.4 Physiologically based pharmacokinetic (PBPK) intestine models: (a) the traditional model or TM and (b) the segregated flow model or SFM, with the intestine as the only elimination tissue. For the SFM, the intestine tissue is divided into the enterocyte (en) region and the serosal (s) region. See text for description of flows, volumes, and assumptions.

by the intestinal or portal venous blood flow, Q_I or Q_{PV}, and V_{intb}, V_{int}, and V_{lumen} represent volumes of the various intestinal subcompartments, intestinal blood, the intestine, and the lumen, respectively. The drug is delivered under constant blood flow (Q_I) into the intestinal blood via the superior mesenteric artery and exits the intestine into the portal vein. The influx of the drug into the intestinal tissue from the blood is characterized by the transport clearance parameter, CL^I_{d1}. Once the drug traverses the basolateral membrane to enter the tissue, it undergoes biotransformation to form metabolites (denoted by the intestinal metabolic clearance, $CL_{int,met1,I}$ and $CL_{int,met2,I}$) or excretion (denoted by intrinsic secretion clearance $CL_{int,sec,I}$) or may be effluxed back to the circulation (denoted by transport clearance CL^I_{d2}). The absorption rate constant of drug and metabolite from the intestinal lumen is denoted by k_a or $k_a\{mi\}$, and their transit or degradation/metabolism rate constants within the lumen, representing net loss in lumen, are denoted by k_g or $k_g\{mi\}$, to denote an ineffective absorption.

Owing to failure of the TM to predict route-dependent intestinal metabolism, namely little or no metabolism occurring after systemic dosing but notable metabolism following oral dosing, the segregated flow model (SFM) has been subsequently developed (Fig. 16.4b). The development was sparked by observations on morphine (M) glucuronidation to the 3-glucuronide (M3G) in the perfused rat intestine preparation: the lack of [^{3}H]M3G formed after systemic [^{3}H]M administration and the abundance of [^{3}H]M3G (13% dose) formed after [^{3}H]M administered intraduodenally support the hypothesis of route-dependent metabolism [13]. According to the SFM, a reduced blood flow rate perfuses the enterocyte layer, reducing the rate of drug delivery to intestinal enzymes or secretory sites and rendering lower values of intestinal clearance [14]. However, during oral absorption, the entire orally administered dose must traverse the enterocyte layer before the substrate enters the circulation. The differential exposure with the route of administration results in different extents of exsorption and metabolism and contributes to the observation of route-dependent metabolism. The SFM is consistent with intestinal blood patterns of about 60–70% of the intestinal flow [115] perfusing the nonabsorptive and nonmetabolizing serosal and submucosal regions, and only a low, partial flow (~18% [116], 5–7% [117,118], or 10–30% [119,120]) of the intestinal blood perfuses the absorptive and metabolizing enterocyte region where the metabolic enzymes and the transporters are located [14]. The SFM further provides a view that was adopted in commercially available programs such as Simcyp® [121]. As shown in Fig. 16.4b, the parent drug and metabolite are delivered under constant blood flow ($0.9Q_I$) to the serosal tissue, which is characterized by the transport clearance parameter, CL^I_{d3} and $CL^I_{d3}\{mi\}$, respectively. The parent drug and metabolite can also be effluxed back into serosal blood (CL^I_{d4} or $CL^I_{d4}\{mi\}$), respectively.

Utilizing these two models, Sun and Pang [18,122] solved the AUC terms for the parent drug and metabolite (Table 16.4). The solutions for AUC_{po}, $AUC_{po}\{mi\}$, and $AUC_{iv}\{mi\}$ are found to be identical for the TM and SFM, whereas for AUC_{iv}, the solution is similar except that Q_I exists in the solution for the TM and Q_{en} for the SFM. The secretory intestinal intrinsic clearance of the drug ($CL_{int,sec,I}$) is found associated with the term $(1-F_{abs})$, where F_{abs} is the fraction absorbed or $k_a/(k_a + k_g)$. When the absorbed fraction, F_{abs}, is high (~1) due to the high k_a relative to k_g, net secretion is effectively reduced to zero. Moreover, AUC_{po} and AUC_{iv} are found to be inversely related to the sum of $(1 - F_{abs})CL_{int,sec,I}$ and $CL_{int,met,I}$, whereas $AUC_{po}\{mi\}$ and $AUC_{iv}\{mi\}$ are further related inversely to the sum of $(1 - F_{abs}\{mi\})CL_{int,sec,I}\{mi\}$ and

TABLE 16.4 Solutions for AUC_{iv}, AUC_{po}, $AUC_{iv}\{mi\}$, and $AUC_{po}\{mi\}$ for the TM and SFM, with Intestine as the Only Eliminating Organ[a]

AUC Terms	Solutions for the TM and SFM
$AUC_{po}^{TM\&SFM}$	$\dfrac{F_{abs}\,dose_{po}\,CL_{d2}^{I}}{CL_{d1}^{I}\left[(1-F_{abs})\,CL_{int,sec,I}+CL_{int,met1,I}+CL_{int,met2,I}\right]}$
$AUC_{po}\{mi,P\}^{TM\&SFM}$	$\dfrac{Dose_{po}\,F_{abs}\,CL_{int,met1,I}\,CL_{d2}^{I}\{mi\}}{\left[(1-F_{abs})\,CL_{int,sec,I}+CL_{int,met1,I}+CL_{int,met2,I}\right]CL_{d1}^{I}\{mi\}\left[(1-F_{abs}\{mi\})\,CL_{int,sec,I}\{mi\}+CL_{int,met,I}\{mi\}\right]}$
AUC_{iv}^{TM} or AUC_{iv}^{SFM}[b]	$\dfrac{Dose_{iv}\left[CL_{d1}^{I}\left[(1-F_{abs})\,CL_{int,sec,I}+CL_{int,met,I}\right]+Q_I\left[(1-F_{abs})\,CL_{int,sec,I}+CL_{int,met,I}+CL_{d1}^{I}\right]\right]}{Q_I CL_{d1}^{I}\left[(1-F_{abs})\,CL_{int,sec,I}+CL_{int,met,I}+CL_{int,met2,I}\right]}$
$AUC_{iv}\{mi,P\}^{TM\&SFM}$	$\dfrac{Dose_{iv}\,CL_{int,met1,I}\,CL_{d2}^{I}\{mi\}}{[(1-F_{abs})\,CL_{int,sec,I}+CL_{int,met1,I}+CL_{int,met2,I}]CL_{d1}^{I}\{mi\}[(1-F_{abs}\{mi\})\,CL_{int,sec,I}\{mi\}+CL_{int,met,I}\{mi\}]}$
CL_{iv}^{TM} or CL_{iv}^{SFM}[b]	$\dfrac{Q_I CL_{d1}^{I}[(1-F_{abs})\,CL_{int,sec,I}+CL_{int,met,I}+CL_{int,met2,I}]}{CL_{d1}^{I}[(1-F_{abs})\,CL_{int,sec,I}+CL_{int,met,I}]+Q_I\left((1-F_{abs})\,CL_{int,sec,I}+CL_{int,met,I}+CL_{d1}^{I}\right)}$

[a]For the SFM, Q_I is Q_{en}.
[b]The flow rate term is Q_{en} for the SFM.
Source: From Sun and Pang [18] with permission.

$CL_{int,met,I}\{mi\}$. Owing to the effective modulation of absorption on $CL_{int,sec,I}$ by F_{abs}, changes in $CL_{int,met,I}$ would exert a greater effect on drug bioavailability compared to $CL_{int,sec,I}$ [122]. The difference in flow between models imparts a substantial influence on the intestinal clearance of flow-limited substrates. The SFM predicts a markedly higher extent of intestinal metabolism for oral compared to intravenous dosing, and the TM predicts a higher intestinal metabolism compared to that for the SFM.

Owing to the varying segmental distributions of absorptive and secretory transporters and metabolic enzymes along the small intestine, the single intestinal compartments of the TM and SFM have been expanded into three equal segmental compartments, segmental, TM and the segmental, SFM [123]. These advanced PBPK models have been applied to predict the impact of metabolic and transporter activities in different segments of the intestine on the intestinal drug clearance and oral drug availability [123].

16.5.3 The Kidney

The kidney is one of the major excretory organs of drugs and metabolite and exhibits a significant capacity to metabolize drugs [12,124,125]. The isolated kidney perfusion is one technique that allows metabolic and excretory events to be examined simultaneously under controlled conditions and described by PBPK modeling. In the PBPK kidney model, the drug is delivered into renal tubular cells by the slightly reduced renal flow (Q_K–GFR) due to removal of plasma water by glomerular filtration (of rate, GFR), and, on the reabsorption of water, the returning flow to the reservoir ($Q_K - Q_U$) is the difference between the renal blood/plasma flow and urinary flow, Q_U (Fig. 16.5). Drug influx and efflux clearances by transporters at the basolateral membrane are described as CL_{in}^{b} and CL_{ef}^{b}, respectively. The drug that is reabsorbed or secreted in the urine compartment by transporters at the apical or luminal membrane with influx and efflux clearances denoted by CL_{in}^{l} and CL_{ef}^{l}, respectively. The drug enters the renal cell either at the basolateral membrane with influx clearance, CL_{in}^{b}, or by reabsorption at the apical membrane (with reabsorptive clearance, CL_{in}^{l}). In the renal tissue, the drug may undergo metabolism denoted by $CL_{int,met,K}$ to form the primary metabolite, Mi, which may undergo transport at the basolateral and apical membranes or further metabolism, denoted by $CL_{in}^{b}\{mi\}$, $CL_{ef}^{b}\{mi\}$, $CL_{in}^{l}\{mi\}$, $CL_{ef}^{l}\{mi\}$, and $CL_{int,met,K}\{mi\}$, respectively.

The kidney PBPK model has been utilized to explain levels of drugs that undergo glomerular filtration, saturable secretion, and/or reabsorption and effects of inhibitors such as probenecid at the basolateral membrane [126–130]. The change in drug reabsorption due to changes in pH was also applied in this model [128]. PBPK models are used to describe renal metabolite formation and immediate excretion and the existence of a nonconstant renal metabolite clearance denoting the kidney as a metabolite formation organ [12,84].

One advantage of using the PBPK kidney modeling approach is the ability to examine the effects of renal transporters and enzymes on renal clearance, CL_R, of a drug. Table 16.5 shows the AUC and CL_R for the kidney with possible alternate pathways for the drug and its metabolite. The basolateral (CL_{in}^{b} and CL_{ef}^{b}) and luminal (CL_{in}^{l} and CL_{ef}^{l}) transporters, the GFR, Q_K, and Q_U all do influence the AUC and CL_R of the drug. The ratio of CL_R and f_PGFR, or fractional excretion (FE) or excretion ratio (ER), denotes whether reabsorption, net filtration, or secretion takes place by deviation of the ratio from below unity to unity or to above unity. When metabolism is relevant,

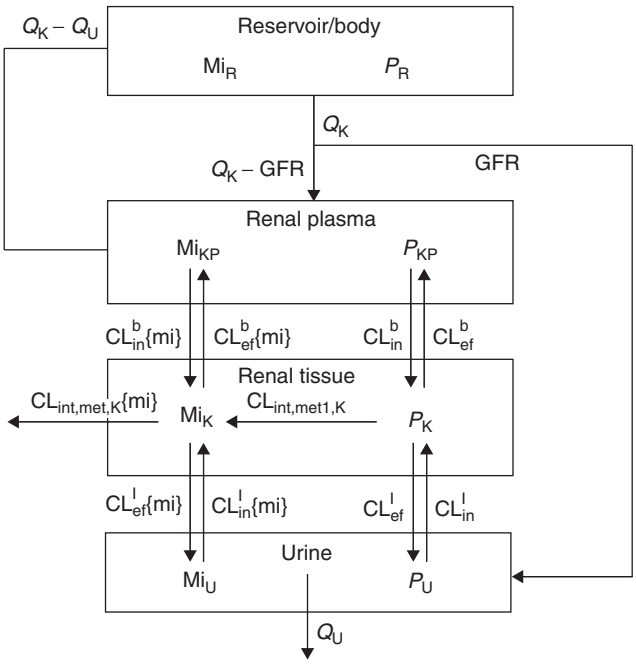

Figure 16.5 Physiologically based pharmacokinetic (PBPK) kidney model, with kidney as the only elimination organ. See text for description of the model.

$CL_{\text{int,met,K}}$ is present in the AUC and CL_R solutions, and the solutions become more complicated (Table 16.5). Indeed, the presence of metabolism as the alternate pathway will affect excretory clearance and further change the FE or ER ratio [91].

Renal PBPK modeling approaches have exploited the concept of drug transport and metabolism to examine the kinetics of a drug and its metabolite(s) in the kidney. In a single-pass kidney perfusion study, the extraction ratio ($E\{\text{mi,P}\} = 0.39$) of hippurate (metabolite formed from its precursor drug, benzoate) was found to differ from the extraction ratio when hippurate ($E\{\text{pmi}\} = 0.24$) was administered [131]. The lower extraction ratio of the administered hippurate was explained by the renal PBPK model, which described a rapid hippurate formation within the renal cells and a high secretion activity of hippurate at the apical membrane; in contrast, the preformed hippurate would first undergo filtration before reaching the peritubular cells and partially evade the high secretory sites.

A renal PBPK model has been applied to examine the metabolism and excretion of enalapril, an ACE inhibitor. In both single-pass and recirculating isolated rat kidney perfusion, a higher extraction ratio of enalaprilat, the dicarboxylic acid metabolite, was observed when the precursor, enalapril, was administered compared to that when preformed enalaprilat was administered. The major reason is the presence of a membrane barrier that retards enalaprilat entry into the kidney and back efflux to blood [12,84,89,125,132]. As a result, preformed enalaprilat was mainly eliminated by GFR. For the metabolite enalaprilat that was formed within the kidney, a much higher and time-dependent renal clearance was observed. The time-dependent excretion clearance

TABLE 16.5 Solutions for AUC_{iv} and CL_R with and without Renal Metabolism in the Kidney Only

AUC and CL_R Terms	Solutions
AUC_{iv} (no metabolism)	$AUC_{iv} = \text{Dose}_{iv} \dfrac{\left\{(Q_K - Q_U)\left[CL^l_{in} CL^b_{ef} + Q_U\left(CL^b_{ef} + CL^l_{ef}\right)\right] + Q_U f_B CL^b_{in} CL^l_{ef}\right\}}{Q_U f_B\left[Q_K CL^b_{in} CL^l_{ef} + \text{GFR}\,(Q_K - Q_U)\left(CL^b_{ef} + CL^l_{ef}\right)\right]}$
CL_R (no metabolism)	$CL_R = \dfrac{Q_U f_B\left[Q_K CL^b_{in} CL^l_{ef} + \text{GFR}\,(Q_K - Q_U)\left(CL^b_{ef} + CL^l_{ef}\right)\right]}{(Q_K - Q_U)\left[CL^l_{in} CL^b_{ef} + Q_U\left(CL^b_{ef} + CL^l_{ef}\right)\right] + Q_U f_B CL^b_{in} CL^l_{ef}}$
AUC_{iv} (with metabolism)	$AUC_{iv} = \dfrac{\text{Dose}_{iv}\left\{(Q_K - Q_U)\left[CL^l_{in}(CL^b_{ef} + CL_{int,met,K}) + Q_U\left(CL^b_{ef} + CL^l_{ef} + CL_{int,met,K}\right)\right] + f_B CL^b_{in}\left[Q_U CL^l_{ef} + CL_{int,met,K}\left(CL^l_{in} + Q_U\right)\right]\right\}}{\text{GFR} f_B\,(Q_K - Q_U)\left[CL_{int,met,K}\left(CL^l_{in} + Q_U\right) + Q_u\left(CL^b_{ef} + CL^l_{ef}\right)\right] + Q_K f_B CL^b_{in}\left[Q_U CL^l_{ef} + CL_{int,met,K}\left(CL^l_{in} + Q_U\right)\right]}$
CL_R (with metabolism)	$CL_R = \dfrac{\text{GFR} f_B\,(Q_K - Q_U)\left[CL_{int,met,K}\left(CL^l_{in} + Q_U\right) + Q_u\left(CL^b_{ef} + CL^l_{ef}\right)\right] + Q_K f_B CL^b_{in}\left[Q_U CL^l_{ef} + CL_{int,met,K}\left(CL^l_{in} + Q_U\right)\right]}{(Q_K - Q_U)\left[CL^l_{in}\left(CL^b_{ef} + CL_{int,met,K}\right) + Q_U\left(CL^b_{ef} + CL^l_{ef} + CL_{int,met,K}\right)\right] + f_B CL^b_{in}\left[Q_U CL^l_{ef} + CL_{int,met,K}\left(CL^l_{in} + Q_U\right)\right]}$

Source: Taken from Pang [86] with permission.

of formed enalaprilat was partially due to the immediate excretion of the enalaprilat that was formed *in situ* in the kidney (the time-dependent component that is dependent on drug concentration in the kidney) and partially due to filtration of the recirculating metabolite (component reflected by preformed metabolite); the sum contributes to the observed renal clearance of the formed metabolite [12,84,125]. This clearance differs from the conventional estimate of the clearance of the preformed metabolite [12].

16.6 WHOLE-BODY PBPK

Whole-body PBPK models provide an understanding of the behaviors of drugs and metabolites based on physiological parameters. Usually, when the intestine, liver, and kidney, major drug eliminating organs/tissues, are included together with highly perfused, poorly perfused, and adipose tissues (Fig. 16.6), mechanisms governing removal and the rate-limiting step (e.g., metabolism by enzymes, influx by transporters, and secretion via apical transporters) are revealed. In this occasion, the renal clearance may be embedded in the blood compartment to describe the parallel loss of drug from

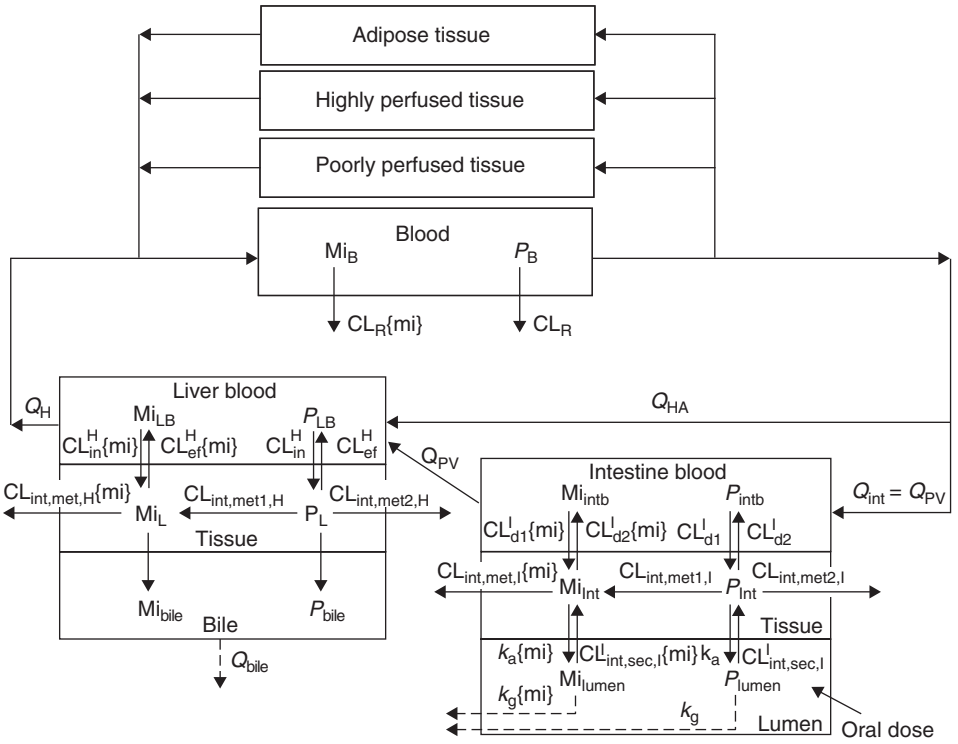

Figure 16.6 Whole-body, physiologically based pharmacokinetic (PBPK) model, with drug and metabolite being excreted by the kidneys with CL_R and $CL_R\{mi\}$, and metabolized either in the intestine or the liver. Sequential metabolism/excretion of the formed metabolite occurs with the organ of formation, and the drug may be further metabolized to other metabolites. Only the intestinal TM is presented here, but the SFM is also considered (Table 16.6). See text for description of the model.

the kidney. The PBPK models provide an account of how the processes of transport and metabolism modulate the kinetics of the drug and its metabolites, and how drug behavior further affects the kinetics of the metabolites (Table 16.6).

The analytical solutions for the AUC and AUC{mi,P} solved for the drug and the formed metabolite divulge how the variables affect the exposure and fates of the drug and the formed metabolite within metabolite formation organs and in blood/plasma (Table 16.6). The solutions reveal that the effect of intestinal secretion is nullified when avid absorption takes place (Table 16.6). It may be further discerned that the ratio of $AUC_{po}\{mi,P\}/AUC_{iv}\{mi,P\}$ pursuant to drug oral and intravenous administration, corrected for dose, yields the fraction of dose absorbed, F_{abs}, into the portal circulation when either the intestine or the liver is the only drug metabolizing organ, and the dose-corrected AUC_{po}/AUC_{iv} yields the systemic availability, F_{sys}. On division of AUC_{po}/AUC_{iv} by $AUC_{po}\{mi,P\}/AUC_{iv}\{mi,P\}$, one obtains the intestinal or hepatic availability (Table 16.6) [18].

16.6.1 Sequential Metabolism and Metabolite Behavior

The PBPK model is particularly pertinent to describe the sequential elimination of the formed metabolite, asserting that the metabolite, formed *in situ* within the formation organ, is subject to immediate excretion or sequential metabolism to form secondary or tertiary metabolites. The reason that estimation of the AUC of the metabolite, AUC{mi, P}, is important because the metabolite may possess active or toxic therapeutics effects [86]. Furthermore, one can take advantage of AUC solutions of the parent drug and the formed metabolites and compare the AUC ratio between intravenous and oral administration to estimate the variables important for drug absorption. Some examples on sequential metabolism are listed in Table 16.7.

The whole-body PBPK model approach clearly explains the influence of transporters and enzymes on the AUCs of the parent drug and its formed metabolites in a route-dependent fashion and that the AUC{pmi} differs from the AUC{mi, P}. Pathways of sequential metabolism of the formed primary metabolite (Mi) can exist either within its organ of formation or in additional eliminating organs. Under this situation, the AUCs and clearances of formed (denoted by subscript, mi) and preformed primary metabolite (denoted by subscript, pmi) differ when there is low permeability of the metabolite, resulting in the delay in the kinetics due to the formation step of the formed metabolite and/or competition for the drug in the same or other organs. These differences have been demonstrated both experimentally and theoretically [15,18,102,122,142–144]. The discrepancy is also caused by differences in enzyme/transporter heterogeneity within the organ involved in formation or further metabolism of Mi [15,18,86,122]. These differences must be borne in mind when the kinetics of the preformed metabolite is used to predict the kinetics of the formed metabolite, especially for MIST.

16.6.2 Examination of Transporter and Enzyme Interplay

Generalized whole-body PBPK models have been developed to describe the impact of transporters and enzymes on the PK of the parent drug and the disposition of formed metabolites. Not until recently, these models lack the appropriate subcompartments within the organs to describe the influence of different transporters and enzymes or the parent drug and metabolites. Sun and Pang [18] described a whole-body PBPK model

TABLE 16.6 Solutions in the Whole-Body PBPK Model

AUC Solutions	
For Intestinal Metabolism and Renal Excretion Only	
AUC_{iv}	$AUC_{iv} = Dose_{iv} \dfrac{Q_{PV}CL^{I}_{d2} + (Q_{PV} + CL^{I}_{d1})\left[CL_{int,met1,I} + CL_{int,met2,I} + (1 - F_{abs})\,CL_{int,sec,I}\right]}{CL_R\,Q_{PV}CL^{I}_{d2} + \left[CL_R\,Q_{PV} + CL^{I}_{d1}\,(CL_R + Q_{PV})\right]\left[CL_{int,met1,I} + CL_{int,met2,I} + (1 - F_{abs})\,CL_{int,sec,I}\right]}$
$AUC_{iv}\{mi,P\}$	$AUC_{iv}\{mi,P\} = Dose_{iv} \dfrac{CL_{int,met1,I}\,Q_{PV}CL^{I}_{d1}}{CL_R\,Q_{PV}CL^{I}_{d2} + \left[CL_R\,Q_{PV} + CL^{I}_{d1}\,(CL_R + Q_{PV})\right]\left[CL_{int,met1,I} + CL_{int,met2,I} + (1 - F_{abs})\,CL_{int,sec,I}\right]} \times \dfrac{Q_{PV}CL^{I}_{d2}\{mi\}}{CL_{R\{mi\}}\,Q_{PV}CL^{I}_{d2}\{mi\} + \left[CL_R\{mi\}\,Q_{PV} + CL^{I}_{d1}\{mi\}\,(CL_R\{mi\} + Q_{PV})\right]\left[CL_{int,met,I}\{mi\} + (1 - F_{abs}\{mi\})\,CL_{int,sec,I}\{mi\}\right]}$
AUC_{po}	$AUC_{po} = Dose_{po} \dfrac{F_{abs}\,Q_{PV}CL^{I}_{d2}}{CL_R\,Q_{PV}CL^{I}_{d2} + \left[CL_R\,Q_{PV} + CL^{I}_{d1}\,(CL_R + Q_{PV})\right]\left[CL_{int,met1,I} + CL_{int,met2,I} + (1 - F_{abs})\,CL_{int,sec,I}\right]}$
$AUC_{po}\{mi,P\}$	$AUC_{po}\{mi,P\} = Dose_{po} \dfrac{F_{abs}CL_{int,met1,I}\left[CL^{I}_{d1}\,(CL_R + Q_{PV}) + CL_R\,Q_{PV}\right]}{CL_R\,Q_{PV}CL^{I}_{d2} + \left[CL^{I}_{d1}\,(CL_R + Q_{PV}) + CL_R\,Q_{PV}\right]\left[CL_{int,met1,I} + CL_{int,met2,I} + (1 - F_{abs})\,CL_{int,sec,I}\right]} \times \dfrac{Q_{PV}CL^{I}_{d2}\{mi\}}{CL_R\{mi\}\,Q_{PV}CL^{I}_{d2}\{mi\} + \left[CL_R\{mi\}\,Q_{PV} + CL^{I}_{d1}\{mi\}\,(CL_R\{mi\} + Q_{PV})\right]\left[CL_{int,met,I}\{mi\} + (1 - F_{abs}\{mi\})\,CL_{int,sec,I}\{mi\}\right]}$

(*continued overleaf*)

TABLE 16.6 (*Continued*)

AUC Solutions	
For Hepatic Metabolism ($Q_H = Q_{PV} + Q_{HA}$) and Renal Excretion Only	
AUC_{iv}	$AUC_{iv} = Dose_{iv} \frac{[Q_H(CL_{ef}^H + CL_{int,H}) + CL_{in}^H CL_{int,H}]}{CL_R Q_H(CL_{ef}^H + CL_{int,H}) + CL_{in}^H CL_{int,H}(CL_R + Q_H)}$
$AUC_{iv}\{mi,P\}$	$AUC_{iv}\{mi,P\} = Dose_{iv} \frac{Q_H CL_{in}^H CL_{int,met1,H}}{CL_R Q_H(CL_{ef}^H + CL_{int,H}) + CL_{in}^H CL_{int,H}(CL_R + Q_H)} \times \frac{Q_H CL_{ef}^H\{mi\}}{CL_R\{mi\} Q_H(CL_{ef}^H\{mi\} + CL_{int,H}\{mi\}) + CL_{in}^H\{mi\} CL_{int,H}\{mi\}(CL_R\{mi\} + Q_H)}$
AUC_{po}	$AUC_{po} = Dose_{po} \frac{F_{abs} Q_H(CL_{ef}^H + CL_{int,H})}{CL_R Q_H(CL_{ef}^H + CL_{int,H}) + CL_{in}^H CL_{int,H}(CL_R + Q_H)}$
$AUC_{po}\{mi,P\}$	$AUC_{po}\{mi,P\} = Dose_{po} \frac{F_{abs} Q_H CL_{in}^H CL_{int,met1,H}(CL_R + Q_H)}{CL_R Q_H(CL_{ef}^H + CL_{int,H}) + CL_{in}^H CL_{int,H}(CL_R + Q_H)} \times \frac{CL_{ef}^H\{mi\}}{CL_R\{mi\} Q_H(CL_{d2}^H\{mi\} + CL_{int,H}\{mi\}) + CL_{in}^H\{mi\} CL_{int,H}\{mi\}(CL_R\{mi\} + Q_H)}$

Source: From Sun and Pang [18] with permission.

TABLE 16.7 Examples of PBPK Modeling for Sequential Metabolism

Chemicals and Major Metabolic Pathway of Interest	Applications and Features	References
Nicotine → cotinine→ polar metabolites	• Studied nicotine disposition in SD rats • Described tissue and plasma kinetics of cotinine, a biomarker for exposure to tobacco smoke • Used *in vivo* rat nicotine PK study to validate the predictive power of the PBPK model	134
Butadiene → butadiene monoxide → butadiene monoxide glutathione conjugate	• Examined potential carcinogen effect of butadiene, an environmental air pollutant • Validated PBPK model against published observations on butadiene and butadiene monoxide and liver glutathione kinetics in rats and mice *in vivo* • PBPK model was used to explain species difference in cancer response between mice and rats exposed to butadiene	135,136
Styrene → styrene → styrene-7,8-oxide → styrene-7,8-oxide glutathione conjugate	• Illustrated the carcinogenic potential of styrene due to its active metabolite styrene-7,8-oxide in risk assessment • Included cosubstrate, glutathione, to describe conjugation of styrene-7,8-oxide to its conjugate by glutathione-*S*-transferase	137
Octamethylcyclotetrasiloxane (D_4) → short-chain linear siloxanes	• PBPK of inhalation kinetics of D_4, a silicon fluid, in humans during rest and exercise	138
Uracil → dihydrouracil → β-ureidopropionate → β-alanine	• Described $^{13}CO_2$ exhalation after orally administered [2−^{13}C]uracil • Reported dihydropyrimidine dehydrogenase as the key enzyme of cytotoxicity of 5-FU • Used [2−^{13}C]uracil in identifying patients at risk of 5-FU toxicity	139
Atrazine → chlorotriazines → diaminochlorotriazine → glutathione conjugates	• Described oral absorption and oxidative metabolism of atrazine on the blood time course curves of individual chlorotriazines in rat, and the toxic neuroendocrine effects associated with chlorotriazines exposure but not of the nonchlorinated metabolites	140
Dichloromethane (DCM) → formyl chloride → CO	• Evaluated two different metabolic hypotheses for DCM toxicity using PBPK modeling for *in vivo* inhalation gas uptake data exposure in female B6C3F1 mice	141

Source: Adapted from Fan *et al*. 133.

approach that includes both transporters and enzymes and their impact on the AUC and PK of the parent drug and the formed metabolites. This whole-body PBPK model approach clearly explains the influence of transporters and enzymes on the AUCs of the parent drug and its formed metabolites in a route- and time-dependent fashion (Table 16.6).

There are an increasing number of studies with PBPK modeling that examine effects of the interplay of transporters and enzymes on the blood and target organ exposures of the drug and its metabolites [78]. Watanabe *et al*. [79] reported that changes in pravastatin hepatic uptake greatly altered the plasma concentration but had minimal effect on the concentration in liver, whereas alteration of hepatic efflux transporters would greatly affect liver concentration but not plasma concentration. In another study, Rowland Yeo *et al*. [145] found that enzyme inhibition of triazolam by diltiazem and its metabolite, *N*-desmethyldiltiazem, plays a role in affecting the AUC of triazolam.

16.7 APPLICATIONS OF PBPK MODELS

16.7.1 Prediction of Exposure in Tissue Sites

In principle, PBPK models permit the prediction of the concentration of the parent drug and metabolites in any tissue or target organ. Examples are tumor tissue [146], the fetus [147], the testes [28], or other various tissues [4,134,148,149] within the body, providing additional physiological information and mechanistic answers. In addition, PBPK models are superior over traditional PK models in that they can be used to explain the nonlinear uptake of parent drugs from skin into tissue sites [150], membrane-limited uptake of drugs [151], or the disposition of both the parent drug and its metabolite in tissue sites [152]. Table 16.8 lists examples investigating drug exposure at tissue sites which were described by PBPK models.

16.7.2 Prediction of Pharmacological Activity or Toxicity

PBPK/PD models are also useful for predicting the relationship between drug exposure and pharmacological and/or toxicological effects in target organs to explain pharmacological [154,155] and toxicological outcomes [146,156,157]. By providing a link between tissue concentration and pharmacological and/or toxicological effects, PBPK models can be expanded to form mechanistic PK/PD models [158]. When combined with a mechanistic or empirical PD model (PBPK/PD), the therapeutic outcome or adverse events within a certain population could be predicted before clinical studies. The PBPK/PD model is created when the PBPK model is linked to a pharmacodynamic (PD) model by an equation that reflects the researcher's hypothesis of how the drug participates in the initiation of cellular changes leading to measurable outcomes. The temporal change in the dose metric simulated by the PBPK model is linked with mathematical descriptions of the response process associated with the drug.

Table 16.9 summarizes applications of PBPK/PD model to quantify the relationship between the drug and the pharmacologic effect. A semimechanistic PK–PD model, with incorporation of saturable hepatic elimination on the first-pass extraction as well as a

TABLE 16.8 Examples of Whole-Body PBPK Models that Emphasize Drug Exposure at Tissue Sites

Chemicals	Species	Model	References
5-Flourouraacil (5-FU)	Mouse	Flow-limited model to predict accumulation of 5-FU in human tumor tissues	146
Barbiturates	Rat	Flow-limited compartments for lung, liver, kidney, stomach, pancreas, spleen, gut, muscle, adipose, skin, bone, and heart and membrane-limited compartments in brain and testis barbiturates disposition in different tissues	149
Chlordecone	Rat	Flow-limited model to evaluate the effect of age and dosage on percutaneous absorption and tissue disposition of chlordecone	153
Digoxin	Rat	Flow-limited model to predict the concentrations of digoxin in the heart, liver, skeletal muscle, and plasma	148
Everolimus	Rat	Flow-limited model to predict nonlinear binding of everolimus to red blood cells and tissues, and the highest tissue binding in thymus, skin, and muscle	150
Moxalactam	Rat, dog, and human	Membrane-limited model to explain moxalactam epimerization on the warfarin-binding site of serum albumin	151
Nicotine	Rat	Flow-limited model to predict the nonlinear nicotine elimination in the brain, heart, and lung, suggesting that saturable nicotinic binding sites may be important in nicotine disposition	134
p-Phenylbenzoic acid	Rat	Flow-limited model to predict *p*-phenylbenzoic acid concentration–time profiles in different tissues of the mother and placenta of the fetuses	147
Thiopental	Dog	Flow-limited model to predict thiopental concentrations in blood, viscera, lean tissue, and adipose tissue	4
Tretinoin	Rat, monkey, and human	Flow-limited model to predict tretinoin pharmacokinetics in plasma and different tissues and to extrapolate across species and routes of administration	152

TABLE 16.9 Examples of Whole-Body PBPK/PD Models

Applications and Features		References
Quantified Relationship Between Drug and Effect		
Diisopropylfluorophosphate (DFP)	Effect of DFP on acetylcholinesterase activity	160
Glycyrrhetic acid	Inhibition of 11β-hydroxysteroid dehydrogenase activity	157
Chlorpyrifos	Evaluated the chlorpyrifos toxicity, pharmacokinetics, and tissue cholinesterase inhibition in neonatal and adult rats	161
Carbofuran	Characterized AChE inhibition from carbofuran exposure	162
Predicted Toxicologic Interactions		
Trichloroethylene and 1,1-dichloroethylene	Predicted the toxicologic interactions and define the interaction threshold	163
Kepone and carbon tetrachloride	Predicted the toxicologic interactions and define the interaction threshold	164
Linked Drug Dosimetry with Biological Response		
Trichloroethylene	Evaluated the organ toxicity from oral exposure and inhalation	165
Chlorpyrifos and diazinon	Determined dosimetry and cholinesterase inhibition	161
Diazinon and its metabolites	Determined dosimetry and cholinesterase inhibition	166
Carbaryl and its metabolites	Predicted the carbaryl-induced inhibition of cholinesterase activity	167
Evaluated Organ Toxicity Resulting from Metabolites		
Trichloroethylene	Evaluated the organ toxicity resulting from metabolites	165
Performed Various Forms of Extrapolation		
Acrylamide	Extrapolated data from rodent to human	168,169
Brivaracetam	Extrapolated data from rodent to human	170

higher intrinsic clearance in female patients, resulted in the best fit to the time course of salivary artemisinin concentrations after repeated dosing and the number of parasites in patients treated with the drug [159]. The effect of diisopropylfluorophosphate (DFP) on acetylcholinesterase (AChE) activity in mouse and rat was studied using a PBPK/PD model, which accurately predicted the AChE activity similar to those found *in vivo* based on the blood concentration of DFP [160].

The PBPK/PD model may also be used to evaluate organ toxicity developed from trichloroethylene (TCE) metabolites [165]. To date, there are over 250 scientific research papers (searched via PubMed, PBPK + toxicity) using similar PBPK modeling approaches to predict and explain the toxicity of drugs, environmental chemicals, or its metabolites in animal or human models [171–173]. Table 16.10 lists examples of PBPK models that were used to predict chemical exposure and toxicity *in vivo*. Doerge *et al*. [168] used a PBPK/PD model to translate the findings from rodent neurotoxicity and cancer risks into estimates of risks in human acrylamide exposure through diet. PBPK/PD models are also useful tools for linking drug dosimetry with biological response and for evaluating the risk associated with a given drug exposure. Barton and Clewell [165] used a PBPK/PD model to evaluate eye malformation, liver effects, immunotoxicity, and kidney toxicity from oral exposure and neurological, liver, and kidney effects by inhalation with dose metrics for TCE.

Other studies had estimated toxicological exposures of chemicals and drugs that ranged from phthalate esters found in drinking water to acetonylacetone (a neurotoxic industrial solvent), trace metals such as iodine and chromium, and therapeutic drugs such as digoxin [28,171] in target organs. Using the appropriate physiological parameters, Sweeney *et al*. [180] were able to relate the incidence of liver adenomas and carcinomas to the liver exposure (AUC) of trichloroacetic acid, the toxic metabolite of perchloroethylene (a solvent used in dry cleaning), in a mouse PBPK model. In another toxicological study, a generalized rat whole-body PBPK model, focusing primarily on the liver, examined the involvement of transporters such as Mrp2 on the liver exposure of pentachlorobipenyl, a carcinogenic environmental pollutant and a substrate of Mrp2, and liver carcinogenicity [179]. Toxicologic interactions have been predicted with PBPK/PD modeling that defined the interaction threshold between TCE and 1,1-dichloroethylene (1,1-DCE) [163] and between kepone and carbon tetrachloride (CCl_4) [164].

16.7.3 Effects of Disease States, Pregnancy, Age, and Polymorphism

PBPK modeling approaches in toxicological studies not only focus on exposure of toxicants to healthy adults but also apply to pregnant women [182], children [183], the elderly [184], and the study of genetic polymorphism [185]. PBPK models enable us to evaluate the drug concentration–time profile for any dose and administration route under various physiological conditions: disease state, pregnancy, age, and polymorphism.

There have only been a few studies that relate to PK of drugs in disease states with PBPK modeling. For instance, a PBPK model describing drug kinetics in interstitial fluid in patients with hemorrhagic shock followed by fluid resuscitation was used to evaluate amoxicillin and clavulanate PK [38]. The predictions fit the data well in most instances and were consistent with observed clinical data. A PBPK model adequately described altered midazolam kinetics in elderly patients undergoing

TABLE 16.10 Examples of Whole-Body PBPK Models that Emphasized Drug Toxicity

Chemicals	Species	Model	References
1,1,1,3,3-Pentafluoropropane	Human	Flow-limited model to explain that exposure of 1,1,1,3,3-pentafluoropropane did not result in detection of the metabolite TFPA in urine, suggesting little or no metabolism	174
Arsenic	Mouse	Flow-limited model to explain lack of change in the apparent volume of distribution and tissue-plasma concentration ratios of dimethylarsonic acid after acute and chronic exposure to arsenic	175
Chloroethane	Rat, mouse, human	Flow-limited model to describe different rates of metabolism of chloroethane by glutathione-*S*-transferase in different species, consistent with observations on uterine tumors	25
Dibromoacetic acid	Rat	Membrane-limited model for aggregated tissue, kidney, and liver and liver metabolism of dibromoacetic acid in the toxicity or carcinogenicity in liver	176
Doxorubicin	Dog	Flow-limited model to explain increase in doxorubicin exposure in ABCB1 (null) dog that may lead to GI toxicosis	177
Molinate	Rat, human	Flow-limited model to predict molinate concentrations of the rat blood and testes compartment and testicular toxicity	178
Pentachlorobipenyl (PCB126)	Rat	Flow-limited model to relate AUC of PCB126 in liver and incidence of liver toxicity	179
Phthalic acid diesters	Rat	Flow-limited model to predict that plasma monobutyl phthalate kinetics are sensitive to glucuronidation and enterohepatic recirculation	28
Trichloroacetic acid	Mouse	Flow-limited model to assess at trichloroacetic acid liver (AUC) exposure to risk of liver adenomas and carcinomas	180
Trichloroethylene	Mouse	Flow-limited model to relate extents of metabolites formed from trichloroethylene in liver to cause hepatomegaly	181

orthopedic surgery due to increased f_P values and changes in volume of distribution and clearance as a result of blood loss and significant reduction in albumin concentration when compared to normal patients [37]. When PBPK modeling was applied to predict the outcomes of liver cirrhosis, a disease characterized by a decrease in functional hepatocytes, lowered circulating plasma proteins, and altered hepatic blood flow patterns due to the development of portacaval shunts, some success was found [186].

There have also been attempts to apply a PBPK model to describe the effect of renal failure on drug disposition. Tsuji *et al*. [36] developed a PBPK model to predict elevation of plasma and tissue levels of cefalozin, a β-lactam antibiotic, in rabbits with renal failure, and obtained good correlation between predicted and observed tissue concentrations. A PBPK model proposed by Harrison and Gibaldi [35] was used to assess digoxin PK in the dog with renal failure, and a scale-up with the dog model to human was partially successful in predicting digoxin kinetics in patients with renal failure. In renal disease state, a concomitant reduction in hepatic drug metabolizing activities is often found [187,188]. Moreover, changes in transporters [189,190] were found associated with renal [187] and other diseases: inflammatory bowel diseases and inflammation and infection wherein cyotokines are elevated [190,191]. These accompanying changes in transporter/enzyme function further add complexities to the quantitative prediction with regard to disease-related factors that may limit use of PBPK models, unless the changes are readily identified [192].

Since drug distribution could be altered in pregnancy [193], PBPK models for pregnancy have been used to predict the concentrations of drugs in maternal tissues, the placenta, and/or the fetus [193–198] (Table 16.11). Gabrielsson and colleagues, in particular, had reported on the effects of pregnancy on methadone [197], theophylline [196], pethidine (meperidine) [198], and morphine [195] kinetics in the rat with a PBPK model. Additional reports of PBPK models on pregnancy are listed in Table 16.11.

The prediction of drug exposure in special populations (different age groups including neonates, infants, children, and adult) is often made with PBPK modeling [199–201]. A general PBPK model has been used for the prediction of the PK of model substrates, such as theophylline for CYP1A2 and CYP2E1 and midazolam for CYP3A4, in neonates to young adults by considering the age-related changes in unbound intrinsic hepatic clearances [199], with predictions that were in good agreement with literature data. Furthermore, Edginton *et al*. [200] and Johnson *et al*. [201] had applied PBPK models to assess the age-related physiological changes in younger children for 5 (paracetamol, alfentanil, morphine, theophylline, and levofloxacin) and 11 drugs (midazolam, caffeine, carbamazepam, cisapride, theophylline, diclofenac, omeprazole, *S*-warfarin, phenytoin, gentamycin, and vanvomycin), respectively. The predictions were also in good agreement with observed data and showed that the PBPK models are superior to the method of allometric scaling. Thompson *et al*. [202] further reviewed a physiological database useful for PBPK modeling of the healthy and impaired elderly population.

In addition to the above conditions, PBPK models have also been used to simulate effects of genetic variations [79] and enzyme/transporter heterogeneity [92,95] on drug disposition in eliminating organs and the consequences on pharmacological and toxicological effects [39]. Differences in metabolism due to enzyme abundance (e.g., in the case of CYP2D6 poor metabolizers) or differences in intrinsic enzyme activities (e.g., CYP2C9 variants) could be included in PBPK modeling. Inoue *et al*. [203] had found

TABLE 16.11 Examples for Whole-Body PBPK Model for Pregnancy

Drug	Model	Species	References
Morphine	Flow limited for all tissue; membrane limited (fetus)	Rat	196
Methadone	Flow limited for all tissue; membrane-limited compartments for maternal brain/fetus	Rat, human	197
Pethidine (meperidine)	Flow limited for all tissue; membrane limited for fetus	Rat, human	198
p-Phenylbenzoic acid	Flow limited for some tissue; membrane limited for placenta, brain, gut, spleen, muscle, fat, and skin	Rat	147
Tetracycline	Flow limited for all tissues	Rat	194
Theophylline	Flow limited for all tissue; membrane-limited compartments for maternal brain/fetus	Rat	195

ethnic differences in the *in vivo* clearances of alprazolam, caffeine, chlorozoxazone, cyclosporine, midazolam, omeprazole, sildenafil, tolbutamide, triazolam, *S*-warfarin, and zolpidem with the virtual clinical simulator, Simcyp®, which contains background information on the abundance of various P450s and different population distributions of their alleles to account for genetic and ethnic differences in metabolism. The interesting phenomenon is well described by Dickinson *et al*. [204] using the Simcyp® simulator to predict the impact of genetic polymorphism of CYP2C9 on the PK and PD of *S*-warfarin. Recently, a study on genetic polymorphism of the anionic transporter organic anion transporting polypeptide 1B1 (OATP1B1) examined pravastatin plasma concentrations with PBPK modeling and showed sensitivity of systemic exposure of pravastatin to hepatic uptake [39].

16.7.4 Drug–Drug Interactions

The accurate prediction of potential risks for DDIs is important because DDIs are responsible for reduced efficacy or increased adverse events. DDIs usually result from the induction or inhibition of metabolic enzymes, mostly P450s, or transporters, or from a change in protein binding. Inhibition may involve either simple competitive or time-dependent (mechanism-based) inhibitory kinetics, the latter of which involves destruction of the enzyme/transporter that leads to a reduction in metabolism/transport [17]. Induction of the enzyme/transporter usually involves transcriptional and translational changes that lead to new protein synthesis. Alternately, changes in endogenous substrates, for example, cytokines, or ligands of nuclear receptors can also affect enzyme and transporter levels [190].

A general equation exists for the AUC ratio in the presence of the interactant (or perpetrator) and under control conditions ($AUC_{(I)}/AUC_{(C)}$) to reflect inhibition or

induction of a victim drug:

$$\frac{\mathrm{AUC}_{(\mathrm{I})}}{\mathrm{AUC}_{(\mathrm{C})}} = \frac{1}{\left(\dfrac{f_{\mathrm{m}} f_{\mathrm{m,CYP}}}{\left(\dfrac{\mathrm{CL}_{\mathrm{int(C)}}}{\mathrm{CL}_{\mathrm{int(I)}}}\right)}\right) + (1 - f_{\mathrm{m}} \cdot f_{\mathrm{m,CYP}})} \tag{16.17}$$

where f_{m}, $f_{\mathrm{m,cyp}}$, $\mathrm{CL}_{\mathrm{int(C)}}$, and $\mathrm{CL}_{\mathrm{int(I)}}$ are the fraction of the dose metabolized by all P450 isoforms, the fraction of the dose metabolized by each specific P450 enzyme, and the intrinsic clearances under control and inhibited conditions, respectively [205–207].

For reversible metabolism, the ratio of $\mathrm{CL}_{\mathrm{int(C)}}/\mathrm{CL}_{\mathrm{int(I)}}$ equals

$$\frac{\mathrm{CL}_{\mathrm{int(C)}}}{\mathrm{CL}_{\mathrm{int(I)}}} = 1 + \frac{[I]}{K_{\mathrm{I}}} \tag{16.18}$$

where $[I]$ is the inhibitor concentration and K_I is the inhibition constant.

For time-dependent (mechanism-based) inhibition, the ratio of $\mathrm{CL}_{\mathrm{int(C)}}/\mathrm{CL}_{\mathrm{int(I)}}$ equals

$$\frac{\mathrm{CL}_{\mathrm{int(C)}}}{\mathrm{CL}_{\mathrm{int(I)}}} = 1 + \frac{k_{\mathrm{inact}}}{K_{\mathrm{I}}} \frac{[\mathrm{I}]}{k_{\mathrm{deg}}} \tag{16.19}$$

where k_{inact} and k_{deg} are the rate constants for inactivation and degradation of the enzyme, respectively [208,209].

For induction, the ratio of $\mathrm{CL}_{\mathrm{int(C)}}/\mathrm{CL}_{\mathrm{int(I)}}$ equals

$$\frac{\mathrm{CL}_{\mathrm{int(C)}}}{\mathrm{CL}_{\mathrm{int(I)}}} = 1 + \frac{E_{\mathrm{max}}[I]}{\mathrm{EC}_{50} + [I]} \tag{16.20}$$

where E_{max} and EC_{50} are the maximum induction activity and the concentration of inducer associated with half maximum induction, respectively [210]

These types of static AUC comparisons, however, have been criticized since the inhibitor concentration or $[I]$, taken as C_{max} or unbound C_{max} [211], does not reflect the concentrations of drug and interactant at the site of interaction of the enzyme/transporter. Furthermore, the interaction may lead to changes in protein levels of the enzymes/transporters or consequences on the synthesis and degradation rate. Under the same circumstances, the concentration of the interactant may also be changed.

DDI predictions with the use of PBPK modeling on reversible inhibition afford more accurate predictive ability than conventional methods (Eq. 16.18) that fail to describe the $[\mathrm{I}]/K_{\mathrm{I}}$ ratio, given that [I], or the concentration of the inhibitor at the enzyme site, is not static but changes with time and mutual inhibition. Some studies included PBPK models for simulating the changes in drug kinetics with reversible DDIs [211–213]. Furthermore, a whole-body PBPK approach based on a gut compartmental absorption and transit (CAT) model showed improved predictions on DDIs of midazaolam, the CYP3A4 substrate, which was coadministered with ketoconazole or verapamil [214]. In comparison, the conventional, static approach with the use of $[\mathrm{I}]/K_{\mathrm{I}}$ overpredicted levels of midazolam, whereas predictions by the PBPK model were superior (within

TABLE 16.12 Use of Whole-Body PBPK Models for DDIs

Drug	Combination Drug (Inhibitor)	Species	References
2′,3′-Dideoxyinosine	Pentamide	Rat and human	212
Ethoxybenzamide	Salicylamide	Rabbit	215
Midazolam	Clarithromycin	Human	216
Midazolam	Ketoconazole or verapamil	Human	214
Ritonavir, amprenavir, saquinavir, nelfinavir, and indinavir in multiple therapy	Ritonavir, amprenavir, saquinavir, nelfinavir, and indinavir	Rat	217
Tolbutamide	Sulfaphenazole, sulfadimethoxine, and sulfamethoxazole	Rat	40
Triazolam	Erythromycin	Human	211
Warfarin	Bromosulfophthalein	Rat	218

twofold for AUC and C_{max}), regardless of administration route, dosage, and/or coadministration with an inhibitor [214]. These examples are summarized in Table 16.12.

PBPK models that entail dynamic changes in concentration of the perpetrator and victim drug have also been proposed [145,216,217,219]. For example, a simplified PBPK model incorporating two elimination pathways for intestinal and hepatic metabolism of HIV protease inhibitors, including ritonavir, amprenavir, saquinavir, nelfinavir, and indinavir, was constructed to describe multiple HIV therapy and, subsequently, the interaction due to multitherapy with the protease inhibitors [217]. The observed and predicted AUCs according to the PBPK model were in good agreement after oral administration in rats. Zhang *et al*. [219] described changes in intestinal and hepatic P450 protein levels together with changes in activity toward midazolam metabolism due to the mechanism-based inhibition by diltiazem and its major metabolite and predicted the transient and dynamic changes. Quinney *et al*. [216] developed a simple PBPK model, incorporating hepatic and intestinal metabolism by CYP3A and non-CYP3A4 mechanisms, to predict the mechanism-based inhibition of clarithromycin on midazolam metabolism and explained the nonlinear PK of clarithromycin. In another study, Rowland Yeo *et al*. [145] found that the simultaneous competitive and time-dependent enzyme inhibition of triazolam by diltiazem and its metabolite, *N*-desmethyldiltiazem, played a significant role in altering triazolam blood AUC. Clearly, the impact of transporters and enzymes on the exposure of drugs and its metabolite in plasma and target organs are avidly being examined by whole-body PBPK models. Their inclusion, especially under conditions of prolonged inhibition [220], needs to be further investigated.

16.8 CONCLUSIONS

PBPK models are comprehensive models that consider the physiology, anatomy, and biochemistry of the body as well as physicochemical properties of the drug and metabolite. The understanding of absorptive, distribution, metabolic, and excretory

processes through fitting and simulation of concentration–time profiles of plasma and target tissues in generic PBPK models, as discussed in this chapter, allows one to make predictions in target sites and allows proper projection of the effects of age, pregnancy, disease states, and DDIs. Currently, there is an impetus for pharmaceutical industry and FDA to utilize PBPK modeling and commercialized software in drug development and for the prediction of DDIs, genetic polymorphism, and disease states, with animal and *in vitro* studies for the scale-up of transporter and enzyme function to predict transport and metabolic activities in man *in vivo*. These activities have greatly facilitated an understanding of processes affecting the concentration time course, AUC, and clearance of drugs and their metabolites. The increasing use of PBPK modeling in drug development, clinical pharmacology, and risk assessment is a clear testament of the great utility of PBPK modeling in pharmaceutical research.

REFERENCES

1. Gibaldi M, Perrier D. Pharmacokinetics. 2nd ed. New York: Marcel Dekker; 1982.
2. Pang KS, Durk MR. Physiologically-based pharmacokinetic (PBPK) modeling of metabolites. J Pharmacokinet Pharmacodyn 2010;37:591–615.
3. Teorell T. Kinetics of distribution of substances administered to the body. Arch Int Pharmacodyn Ther 1937;57:205–225.
4. Bischoff KB, Dedrick RL. Thiopental pharmacokinetics. J Pharm Sci 1968;57:1346–1351.
5. Zaharko DS, Dedrick RL, Bischoff KB, *et al*. Methotrexate tissue distribution: prediction by a mathematical model. J Natl Cancer Inst 1971;46:775–784.
6. Bischoff KB, Dedrick RL, Zaharko DS, *et al*. Methotrexate pharmacokinetics. J Pharm Sci 1971;60:1128–1133.
7. Dedrick RL. Animal scale up. J Pharmacokinet Biopharm 1973;1:435–461.
8. Boxenbaum H, Ronfeld R. Interspecies pharmacokinetic scaling and the Dedrick plots. Am J Physiol 1983;245:R768–R775.
9. Rowland M, Benet LZ, Graham GG. Clearance concepts in pharmacokinetics. J Pharmacokinet Biopharm 1973;1:123–136.
10. Pang KS, Rowland M. Hepatic clearance of drugs. I. Theoretical considerations of a "well-stirred" model and a "parallel tube" model. Influence of hepatic blood flow, plasma and blood cell binding, and the hepatocellular enzymatic activity on hepatic drug clearance. J Pharmacokinet Biopharm 1977;5:625–653.
11. Hekman P, van Ginneken CA. Simultaneous kinetic modelling of plasma levels and urinary excretion of salicyluric acid, and the influence of probenecid. Eur J Drug Metab Pharmacokinet 1983;8:239–249.
12. de Lannoy IA, Nespeca R, Pang KS. Renal handling of enalapril and enalaprilat: studies in the isolated red blood cell-perfused rat kidney. J Pharmacol Exp Ther 1989;251:1211–1222.
13. Doherty MM, Pang KS. Route-dependent metabolism of morphine in the vascularly perfused rat small intestine preparation. Pharm Res 2000;17:291–298.
14. Cong D, Doherty M, Pang KS. A new physiologically based, segregated-flow model to explain route-dependent intestinal metabolism. Drug Metab Dispos 2000;28:224–235.
15. Pang KS, Morris ME, Sun H. Formed and preformed metabolites: facts and comparisons. J Pharm Pharmacol 2008;60:1247–1275.
16. Pang KS, Maeng HJ, Fan J. Interplay of transporters and enzymes in drug and metabolite processing. Mol Pharm 2009;6:1734–1755.
17. Pang KS, Rodrigues AD, Peter RM. Enzyme- and transporter-based drug-drug interactions: progress and future challenges. New York: Springer; 2010.

18. Sun H, Pang KS. Physiological modeling to understand the impact of enzymes and transporters on drug and metabolite data and bioavailability estimates. Pharm Res 2010; 27:1237–1254.
19. Nestorov IA, Aarons LJ, Arundel PA, *et al*. Lumping of whole-body physiologically based pharmacokinetic models. J Pharmacokinet Biopharm 1998;26:21–46.
20. Rowland M, Balant L, Peck C. Physiologically based pharmacokinetics in drug development and regulatory science: a workshop report. AAPS J 2004;6:56–67.
21. Germani M, Crivori P, Rocchetti M, *et al*. Evaluation of a basic physiologically based pharmacokinetic model for simulating the first-time-in-animal study. Eur J Pharm Sci 2007;31:190–201.
22. Lavé T, Parrott N, Grimm HP, *et al*. Challenges and opportunities with modelling and simulation in drug discovery and drug development. Xenobiotica 2007;37:1295–1310.
23. Gargas ML, Tyler TR, Sweeney LM, *et al*. A toxicokinetic study of inhaled ethylene glycol monomethyl ether (2-ME) and validation of a physiologically based pharmacokinetic model for a pregnant rat and human. Toxicol Appl Pharmacol 2000;165:53–62.
24. Gargas ML, Tyler TR, Sweeney LM, *et al*. A toxicokinetic study of inhaled ethylene glycol ethyl ether acetate and validation of a physiologically based pharmacokinetic model for at and human. Toxicol Appl Pharmacol 2000;165:63–73.
25. Gargas ML, Sweeney LM, Himmelstein MW, *et al*. Physiologically based pharmacokinetic modeling of chloroethane disposition in mice, rats, and women. Toxicol Sci 2008;104:54–66.
26. Dobrev ID, Anderson ME, Yang YSH. *In silico* toxicology: simulating interaction thresholds for human exposure to mixtures of trichloroethylene, tetrachloroethylene, and 1,1,1-trichloroethane. Environ Health Perspect 2002;110:1031–1039.
27. Sweeney L, Andersen ME, Gargas ML. Ethyl acrylate risk assessment with a hybrid computational fluid dynamics and physiologically based nasal dosimetry model. Toxicol Sci 2004;79:394–403.
28. Clewell RA, Kremer JJ, Williams CC, *et al*. Tissue exposures to free and glucuronidated monobutylyphthalate in the pregnant and fetal rat following exposure to di-N-butylphthalate: evaluation with a PBPK model. Toxicol Sci 2008;103:241–259.
29. Chiu WA, Barton HA, DeWoskin RS, *et al*. Evaluation of physiologically based pharmacokinetic models for use in risk assessment. J Appl Toxicol 2007;27:218–237.
30. Rowland M. Physiologic pharmacokinetic models and interanimal species scaling. Pharmacol Ther 1985;29:49–68.
31. Kawai R, Mathew D, Tanaka C, *et al*. Physiologically based pharmacokinetics of cyclosporine A: extension to tissue distribution kinetics in rats and scale-up to human. J Pharmacol Exp Ther 1998;287:457–468.
32. Nestorov I. Whole body pharmacokinetic models. Clin Pharmacokinet 2003;42:883–908.
33. Luttringer O, Theil FP, Poulin P, *et al*. Physiologically based pharmacokinetic (PBPK) modeling of disposition of epiroprim in humans. J Pharm Sci 2003;92:1990–2007.
34. Brightman FA, Leahy DE, Searle GE, *et al*. Application of a generic physiologically based pharmacokinetic model to the estimation of xenobiotic levels in rat plasma. Drug Metab Dispos 2006;34:84–93.
35. Harrison LI, Gibaldi M. Physiologically based pharmacokinetic model for digoxin disposition in dogs and its preliminary application to humans. J Pharm Sci 1977;66:1679–1683.
36. Tsuji A, Nishide K, Minami H, *et al*. Physiologically based pharmacokinetic model for cefazolin in rabbits and its preliminary extrapolation to man. Drug Metab Dispos 1985;13:729–739.
37. Bjorkman S, Wada DR, Berling BM, *et al*. Prediction of the disposition of midazolam in surgical patients by a physiologically based pharmacokinetic model. J Pharm Sci 2001; 90:1226–1241.

38. Tod M, Lagneau F, Jullien V, *et al*. A physiological model to evaluate drug kinetics in patients with hemorrhagic shock followed by fluid resuscitation. Pharm Res 2008; 25:1431–1439.
39. Watanabe T, Kusuhara H, Maeda K, *et al*. Physiologically based pharmacokinetic modeling to predict transporter-mediated clearance and distribution of pravastatin in humans. J Pharmacol Exp Ther 2009;328:652–662.
40. Sugita O, Sawada Y, Sugiyama Y, *et al*. Physiologically based pharmacokinetics of drug-drug interaction: a study of tolbutamide-sulfonamide interaction in rats. J Pharmacokinet Biopharm 1982;10:297–316.
41. Perl W, Chinard FP. A convection-diffusion model of indicator transport through an organ. Circ Res 1968;22:273–298.
42. Roberts MS, Rowland M. Hepatic elimination–dispersion model. J Pharm Sci 1985;74:585–587.
43. Davies B, Morris T. Physiological parameters in laboratory animals and humans. Pharm Res 1993;10:1093–1095.
44. Kawahara M, Sakata A, Miyashita T, *et al*. Physiologically based pharmacokinetics of digoxin in mdr1a knockout mice. J Pharm Sci 1999;88:1281–1287.
45. Jusko WJ, Gretch M. Plasma and tissue protein binding of drugs in pharmacokinetics. Drug Metab Rev 1976;5:43–140.
46. Gillette JR. Overview of drug-protein binding. Ann N Y Acad Sci 1973;226:6–17.
47. Øie S, Levy G. Effect of plasma protein binding on elimination of bilirubin. J Pharm Sci 1975;64:1433–1434.
48. Wilkinson GR, Shand DG. Commentary: a physiological approach to hepatic drug clearance. Clin Pharmacol Ther 1975;18:377–390.
49. Coffey JJ, Bullock FJ, Schoenemann PT. Numerical solution of nonlinear pharmacokinetic equations: effects of plasma protein binding on drug distribution and elimination. J Pharm Sci 1971;60:1623–1628.
50. Yang F, Tong X, McCarver DG, *et al*. Population-based analysis of methadone distribution and metabolism using an age-dependent physiologically based pharmacokinetic model. J Pharmacokinet Pharmacodyn 2006;33:485–518.
51. Lin JH, Sugiyama Y, Awazu S, *et al*. *In vitro* and *in vivo* evaluation of the tissue-to-blood partition coefficient for physiological pharmacokinetic models. J Pharmacokinet Biopharm 1982;10:637–647.
52. Poulin P, Krishnan K. A tissue composition-based algorithm for predicting tissue:air partition coefficients of organic chemicals. Toxicol Appl Pharmacol 1996;136:126–130.
53. Poulin P, Theil FP. Prediction of pharmacokinetics prior to *in vivo* studies. 1. Mechanism-based prediction of volume of distribution. J Pharm Sci 2002;91:129–156.
54. Sato A, Nakajima T. Partition coefficients of some aromatic hydrocarbons and ketones in water, blood and oil. Br J Ind Med 1979;36:231–234.
55. Andersen ME, Clewell HJ 3rd, Gargas ML, *et al*. Physiologically based pharmacokinetics and the risk assessment process for methylene chloride. Toxicol Appl Pharmacol 1987;87:185–205.
56. Murphy JE, Janszen DB, Gargas ML. An *in vitro* method for determination of tissue partition coefficients of non-volatile chemicals such as 2,3,7,8-tetrachlorodibenzo-*p*-dioxin and estradiol. J Appl Toxicol 1995;15:147–152.
57. Chen HS, Gross JF. Estimation of tissue-to-plasma partition coefficients used in physiological pharmacokinetic models. J Pharmacokinet Biopharm 1979;7:117–125.
58. Davis NR, Mapleson WW. A physiological model for the distribution of injected agents, with special reference to pethidine. Br J Anaesth 1993;70:248–258.
59. Bjorkman S. Prediction of the volume of distribution of a drug: which tissue-plasma partition coefficients are needed? J Pharm Pharmacol 2002;54:1237–1245.

60. Khor SP, Bozigian H, *et al*. Potential error in the measurement of tissue to blood distribution coefficients in physiological pharmacokinetic modeling. Residual tissue blood. II. Distribution of phencyclidine in the rat. Drug Metab Dispos 1991;19:486–490.
61. Poulin P, Theil FP. A priori prediction of tissue:plasma partition coefficients of drugs to facilitate the use of physiologically-based pharmacokinetic models in drug discovery. J Pharm Sci 2000;89:16–35.
62. Poulin P, Schoenlein K, Theil FP. Prediction of adipose tissue: plasma partition coefficients for structurally unrelated drugs. J Pharm Sci 2001;90:436–447.
63. Rodgers T, Rowland M. Mechanistic approaches to volume of distribution predictions: understanding the processes. Pharm Res 2007;24:918–933.
64. Rodgers T, Leahy D, Rowland M. Physiologically based pharmacokinetic modeling 1: predicting the tissue distribution of moderate-to-strong bases. J Pharm Sci 2005;94:1259–1276.
65. Rodgers T, Rowland M. Physiologically based pharmacokinetic modelling 2: predicting the tissue distribution of acids, very weak bases, neutrals and zwitterions. J Pharm Sci 2006;95:1238–1257.
66. Bjorkman S, Wada DR, Stanski DR, *et al*. Comparative physiological pharmacokinetics of fentanyl and alfentanil in rats and humans based on parametric single-tissue models. J Pharmacokinet Biopharm 1994;22:381–410.
67. Austin RP, Barton P, Cockroft SL, *et al*. The influence of nonspecific microsomal binding on apparent intrinsic clearance, and its prediction from physicochemical properties. Drug Metab Dispos 2002;30:1497–1503.
68. Hallifax D, Houston JB. Letter to the Editor. Binding of drugs to hepatic microsomes: comment and assessment of current prediction methodology with recommendation for improvement. Drug Metab Dispos 2006;34:724–726.
69. Kilford PJ, Gertz M, Houston JB, *et al*. Hepatocellular binding of drugs: correction for unbound fraction in hepatocyte incubations using microsomal binding or drug lipophilicity data. Drug Metab Dispos 2008;36:1194–1197.
70. Gillette JR. Factors affecting drug metabolism. Ann N Y Acad Sci 1971;179:43–66.
71. Iwatsubo T, Hirota N, Ooie T, *et al*. Prediction of *in vivo* drug metabolism in the human liver from *in vitro* metabolism data. Pharmacol Ther 1997;73:147–171.
72. Rostami-Hodjegan A, Tucker GT. Simulation and prediction of *in vivo* drug metabolism in human populations from *in vitro* data. Nat Rev Drug Discov 2007;6:140–148.
73. Stringer R, Nicklin PL, Houston JB. Reliability of human cryopreserved hepatocytes and liver microsomes as *in vitro* systems to predict metabolic clearance. Xenobiotica 2008;38:1313–1329.
74. Stringer RA, Strain-Damerell C, Nicklin P, *et al*. Evaluation of recombinant cytochrome p450 enzymes as an *in vitro* system for metabolic clearance predictions. Drug Metab Dispos 2009;37:1025–1034.
75. Kamiie J, Ohtsuki S, Iwase R, *et al*. Quantitative atlas of membrane transporter proteins: development and application of a highly sensitive simultaneous LC/MS/MS method combined with novel in-silico peptide selection criteria. Pharm Res 2008;25:1469–1483.
76. Li N, Zhang Y, Hua F, *et al*. Absolute difference of hepatobiliary transporter multidrug resistance-associated protein (MRP2/Mrp2) in liver tissues and isolated hepatocytes from rat, dog, monkey, and human. Drug Metab Dispos 2009;37:66–73.
77. Kusuhara H, Sugiyama Y. *In vitro-in vivo* extrapolation of transporter-mediated clearance in the liver and kidney. Drug Metab Pharmacokinet 2009;24:37–52.
78. Kusuhara H, Sugiyama Y. Pharmacokinetic modeling of the hepatobiliary transport mediated by cooperation of uptake and efflux transporters. Drug Metab Rev 2010;4:539–550.
79. Watanabe T, Maeda K, Kondo T, *et al*. Prediction of the hepatic and renal clearance of transporter substrates in rats using *in vitro* uptake experiments. Drug Metab Dispos 2009;37:1471–1479.

80. Yanni SB, Augustijns PF, Benjamin DK Jr, *et al*. *In vitro* investigation of the hepatobiliary disposition mechanisms of the antifungal agent micafungin in humans and rats. Drug Metab Dispos 2010;38:1848–1856.
81. Li M, Yuan H, Li N, *et al*. Identification of interspecies difference in efflux transporters of hepatocytes from dog, rat, monkey and human. Eur J Pharm Sci 2008;35:114–126.
82. Pang KS, Gillette JR. Sequential first-pass elimination of a metabolite derived from a precursor. J Pharmacokinet Biopharm 1979;7:275–290.
83. de Lannoy IAM, Pang KS. Effect of diffusional barriers on drug and metabolite kinetics. Drug Metab Dispos 1987;15:51–58.
84. de Lannoy IA, Pang KS. Combined recirculation of the rat liver and kidney: studies with enalapril and enalaprilat. J Pharmacokinet Biopharm 1993;21:423–456.
85. Xu X, Tang BK, Pang KS. Sequential metabolism of salicylamide exclusively to gentisamide 5-glucuronide and not gentisamide sulfate conjugates in single-pass *in situ* perfused rat liver. J Pharmacol Exp Ther 1990;253:965–973.
86. Pang KS. Safety testing of metabolites: Expectations and outcomes. Chem Biol Interact 2009;179:45–59.
87. Pang KS, Cherry WF, Terrell J, *et al*. Disposition of enalapril and its diacid metabolite, enalaprilat, in a perfused rat liver preparation. Presence of a diffusional barrier for enalaprilat into hepatocytes. Drug Metab Dispos 1984;12:309–312.
88. de Lannoy IAM, Pang KS. A commentary: presence of a diffusional barrier on metabolite kinetics. Enalaprilat as a generated *versus* preformed metabolite. Drug Metab Dispos 1986;14:513–520.
89. de Lannoy IA, Barker F 3rd, Pang KS. Formed and preformed metabolite excretion clearances in liver, a metabolite formation organ: studies on enalapril and enalaprilat in the single-pass and recirculating perfused rat liver. J Pharmacokinet Biopharm 1993;21:395–422.
90. Liu L, Pang KS. The roles of transporters and enzymes in hepatic drug processing. Drug Metab Dispos 2005;33:1–7.
91. Sirianni GL, Pang KS. Organ clearance concepts: new perspectives on old principles. J Pharmacokinet Biopharm 1997;25:449–470.
92. Liu L, Pang KS. An integrated approach to model hepatic drug clearance. Eur J Pharm Sci 2006;29:215–230.
93. Tirona RG, Pang KS. Bimolecular glutathione conjugation kinetics of ethacrynic acid in rat liver: *in vitro* and perfusion studies. J Pharmacol Exp Ther 1999;290:1230–1241.
94. Abu-Zahra TN, Pang KS. Effect of zonal transport and metabolism on hepatic removal: enalapril hydrolysis in zonal, isolated rat hepatocytes *in vitro* and correlation with perfusion data. Drug Metab Dispos 2000;28:807–813.
95. Liu L, Mak E, Tirona RG, *et al*. Vascular binding, blood flow, transporter, and enzyme interactions on the processing of digoxin in rat liver. J Pharmacol Exp Ther 2005;315:433–448.
96. Schwab AJ, Barker F III, Goresky CA, *et al*. Transfer of enalaprilat across rat liver cell membranes is barrier-limited. Am J Physiol 1990;258:G461–G475.
97. Doherty MM, Poon K, Tsang C, *et al*. Transport is not rate-limiting in morphine glucuronidation in the single-pass perfused rat liver preparation. J Pharmacol Exp Ther 2006;317:890–900.
98. Tan E, Lu T, Pang KS. Futile cycling of estrone sulfate and estrone in the recirculating perfused rat liver preparation. J Pharmacol Exp Ther 2001;297:423–436.
99. Sun H, Liu L, Pang KS. Increased estrogen sulfation of estradiol 17beta-D-glucuronide in metastatic tumor rat livers. J Pharmacol Exp Ther 2006;319:818–831.
100. Sun H, Zeng Y-Y, Pang KS. Interplay of Phase II enzymes and transporters in futile cycling: influence of multidrug resistance-associated protein 2-mediated excretion of estradiol 17β-D-glucuronide and its 3-sulfate metabolite on net sulfation in perfused TR^- and wistar rat liver preparations. Drug Metab Dispos 2010;38:769–780.

101. Morris ME, Yuen V, Tang BK, *et al*. Competing pathways in drug metabolism. I. Effect of input concentration on the conjugation of gentisamide in the once-through *in situ* perfused rat liver preparation. J Pharmacol Exp Ther 1988;245:614–624.
102. Xu X, Pang KS. Hepatic modeling of metabolite kinetics in sequential and parallel pathways: salicylamide and gentisamide metabolism in perfused rat liver. J Pharmacokinet Biopharm 1989;17:645–671.
103. Suzuki H, Sugiyama Y. Role of metabolic enzymes and efflux transporters in the absorption of drugs from the small intestine. Eur J Pharm Sci 2000;12:3–12.
104. Pang KS. Modeling of intestinal drug absorption: Roles of transporters and metabolic enzymes (For the Gillette Review Series). Drug Metab Dispos 2003;31:1507–1519.
105. Shitara Y, Horie T, Sugiyama Y. Transporters as a determinant of drug clearance and tissue distribution. Eur J Pharm Sci 2006;27:425–446.
106. Dubey RK, Singh J. Localization and characterization of drug-metabolizing enzymes along the villus-crypt surface of the rat small intestine—I. Monooxygenases. Biochem Pharmacol 1988;37:169–176.
107. Ilett KF, Tee LB, Reeves PT, *et al*. Metabolism of drugs and other xenobiotics in the gut lumen and wall. Pharmacol Ther 1990;46:67–93.
108. Hoensch H, Woo CH, Schmid R. Cytochrome P-450 and drug metabolism in intestinal villous and crypt cells of rats: effect of dietary iron. Biochem Biophys Res Commun 1975;65:399–406.
109. Watkins PB, Wrighton SA, Schuetz EG, *et al*. Identification of glucocorticoid-inducible cytochromes P-450 in the intestinal mucosa of rats and man. J Clin Invest 1987;80:1029–1036.
110. Thummel KE, O'Shea D, Paine MF, *et al*. Oral first-pass elimination of midazolam involves both gastrointestinal and hepatic CYP3A-mediated metabolism. Clin Pharmacol Ther 1996;59:491–502.
111. Paine MF, Khalighi M, Fisher JM, *et al*. Characterization of interintestinal and intraintestinal variations in human CYP3A-dependent metabolism. J Pharmacol Exp Ther 1997;283:1552–1562.
112. Thelen K, Dressman JB. Cytochrome P450-mediated metabolism in the human gut wall. J Pharm Pharmacol 2009;61:541–558.
113. Yu LX, Amidon GL. Saturable small intestinal drug absorption in humans: modeling and interpretation of cefatrizine data. Eur J Pharm Biopharm 1998;45:199–203.
114. Ito K, Kusuhara H, Sugiyama Y. Effects of intestinal CYP3A4 and P-glycoprotein on oral drug absorption–theoretical approach. Pharm Res 1999;16:225–231.
115. Schurgers N, de Blaey CJ, Tomlinson E. Non-enhancement of sodium cromoglycate intestinal absorption by quaternary ammonium ions. An effect of salt on ion-pair formation? J Pharm Pharmacol 1984;36:45.
116. MacFerran SN, Mailman D. Effects of glucagon on canine intestinal sodium and water fluxes and regional blood flow. J Physiol 1977;266:1–12.
117. Mailman D. Effects of vasoactive intestinal polypeptide on intestinal absorption and blood flow. J Physiol 1978;279:121–132.
118. Granger DN, Richardson PD, Kvietys PR, *et al*. Intestinal blood flow. Gastroenterology 1980;78:837–863.
119. Svanvik J. Mucosal blood circulation and its influence on passive absorption in the small intestine. An experimental study in the cat. Acta Physiol Scand Suppl 1973;385:1–44.
120. Micflikier AB, Bond JH, Sircar B, *et al*. Intestinal villus blood flow measured with carbon monoxide and microspheres. Am J Physiol 1976;230:916–919.
121. Yang J, Jamei M, Yeo KR, *et al*. Prediction of intestinal first-pass drug metabolism. Curr Drug Metab 2007;8:676–684.

122. Sun H, Pang KS. Disparity in intestine disposition between formed and preformed metabolites and implications: a theoretical study. Drug Metab Dispos 2009;37:187–202.
123. Tam D, Tirona RG, Pang KS. Segmental intestinal transporters and metabolic enzymes on intestinal drug absorption. Drug Metab Dispos 2003;31:373–383.
124. Anders MW. Metabolism of drugs by the kidney. Kidney Int 1980;18:636–647.
125. de Lannoy IA, Hirayama H, Pang KS. A physiological model for renal drug metabolism: enalapril esterolysis to enalaprilat in the isolated perfused rat kidney. J Pharmacokinet Biopharm 1990;18:561–587.
126. Russel FG, Wouterse AC, van Ginneken CA. Physiologically based pharmacokinetic model for the renal clearance of phenolsulfonphthalein and the interaction with probenecid and salicyluric acid in the dog. J Pharmacokinet Biopharm 1987;15:349–368.
127. Russel FG, Wouterse AC, Van Ginneken CA. Physiologically based pharmacokinetic model for the renal clearance of iodopyracet and the interaction with probenecid in the dog. Biopharm Drug Dispos 1989;10:137–152.
128. Boom SP, Moons MM, Russel FG. Renal tubular transport of cimetidine in the isolated perfused kidney of the rat. Drug Metab Dispos 1994;22:148–153.
129. Masereeuw R, Moons MM, Smits P, *et al*. Glomerular filtration and saturable absorption of iohexol in the rat isolated perfused kidney. Br J Pharmacol 1996;119:57–64.
130. Boom SP, Meyer I, Wouterse AC, *et al*. A physiologically based kidney model for the renal clearance of ranitidine and the interaction with cimetidine and probenecid in the dog. Biopharm Drug Dispos 1998;19:199–208.
131. Geng W, Pang KS. Differences in excretion of hippurate, as a metabolite of benzoate and as an administered species, in the single-pass isolated perfused rat kidney explained. J Pharmacol Exp Ther 1999;288:597–606.
132. Schwab AJ, de Lannoy IA, Goresky CA, *et al*. Enalaprilat handling by the kidney: barrier-limited cell entry. Am J Physiol 1992;263:F858–F869.
133. Fan J, Chen S, Chow ECY, *et al*. PBPK modeling of intestinal and liver enzymes and transporters in first-pass drug absorption and metabolite kinetics. Curr Drug Metab 2010;11:743–761.
134. Plowchalk DR, Andersen ME, deBethizy JD. A physiologically based pharmacokinetic model for nicotine disposition in the Sprague-Dawley rat. Toxicol Appl Pharmacol 1992;116:177–188.
135. Johanson G, Filser JG. A physiologically based pharmacokinetic model for butadiene and its metabolite butadiene monoxide in rat and mouse and its significance for risk extrapolation. Arch Toxicol 1993;67:151–163.
136. Johanson G, Filser JG. PBPK model for butadiene metabolism to epoxides: quantitative species differences in metabolism. Toxicology 1996;113:40–47.
137. Csanady GA, Mendrala AL, Nolan RJ, *et al*. A physiologic pharmacokinetic model for styrene and styrene-7,8-oxide in mouse, rat and man. Arch Toxicol 1994;68:143–157.
138. Reddy MB, Andersen ME, Morrow PE, *et al*. Physiological modeling of inhalation kinetics of octamethylcyclotetrasiloxane in humans during rest and exercise. Toxicol Sci 2003;72:3–18.
139. Ito S, Kawamura T, Inada M, *et al*. Physiologically based pharmacokinetic modelling of the three-step metabolism of pyrimidine using C-uracil as an *in vivo* probe. Br J Clin Pharmacol 2005;60:584–593.
140. McMullin TS, Hanneman WH, Cranmer BK, *et al*. Oral absorption and oxidative metabolism of atrazine in rats evaluated by physiological modeling approaches. Toxicology 2007;240:1–14.
141. Evans MV, Caldwell JC. Evaluation of two different metabolic hypotheses for dichloromethane toxicity using physiologically based pharmacokinetic modeling for *in vivo* inhalation gas uptake data exposure in female B6C3F1 mice. Toxicol Appl Pharmacol 2010;244:280–290.

142. St-Pierre MV, Pang KS. Kinetics of sequential metabolism. I. Formation and metabolism of oxazepam from nordiazepam and temazepam in the perfused murine liver. J Pharmacol Exp Ther 1993;265:1429–1436.
143. Pang KS. Acinar factors in drug processing: protein binding, futile cycling and cosubstrate. Drug Metab Rev 1995;27:325–368.
144. Chen J, Pang KS. Effect of flow on first-pass metabolism of drugs: single pass studies on 4-methylumbelliferone conjugation in the serially perfused rat intestine and liver preparations. J Pharmacol Exp Ther 1997;280:24–31.
145. Rowland Yeo K, Jamei M, Yang J, *et al*. Physiologically based mechanistic modelling to predict complex drug-drug interactions involving simultaneous competitive and time-dependent enzyme inhibition by parent compound and its metabolite in both liver and gut—the effect of diltiazem on the time-course of exposure to triazolam. Eur J Pharm Sci 2010;39:298–309.
146. Tsukamoto Y, Kato Y, Ura M, *et al*. Investigation of 5-FU disposition after oral administration of capecitabine, a triple-prodrug of 5-FU, using a physiologically based pharmacokinetic model in a human cancer xenograft model: comparison of the simulated 5-FU exposures in the tumour tissue between human and xenograft model. Biopharm Drug Dispos 2001;22:1–14.
147. Kawahara M, Nanbo T, Tsuji A. Physiologically based pharmacokinetic prediction of p phenylbenzoic acid disposition in the pregnant rat. Biopharm Drug Dispos 1998; 19:445–453.
148. Harrison LI, Gibaldi M. Physiologically based pharmacokinetic model for digoxin distribution and elimination in the rat. J Pharm Sci 1977;66:1138–1142.
149. Blakey GE, Nestorov IA, Arundel P, *et al*. Quantitative structure-pharmacokinetics relationships: I. Development of a whole-body physiologically based model to characterize changes in pharmacokinetics across a homologous series of barbiturates in the rat. J Pharmacokinet Biopharm 1997;25:277–312.
150. Laplanche R, Meno-Tetang GM, Kawai R. Physiologically based pharmacokinetic (PBPK) modeling of everolimus (RAD001) in rats involving non-linear tissue uptake. J Pharmacokinet Biopharm 2007;34:373–400.
151. Yoshikawa T, Oguma T, Ichihashi T, *et al*. Epimerization of moxalactam by albumin and simulation of *in vivo* epimerization by a physiologically based pharmacokinetic model. Chirality 1999;11:309–315.
152. Clewell HJ 3rd, Andersen M, Wills RJ, *et al*. A physiologically based pharmacokinetic model for retinoic acid and its metabolites. J Am Acad Dermatol 1997;36:S77–S85.
153. Heatherington AC, Fisher HL, Sumler MR, *et al*. Percutaneous absorption and disposition of [14 C]chlordecone in young and adult female rats. Environ Res 1998;79:138–155.
154. Sato H, Sugiyama Y, Sawada Y, *et al*. Physiologically based pharmacokinetics of radioiodinated human beta-endorphin in rats. An application of the capillary membrane-limited model. Drug Metab Dispos 1987;15:540.
155. Nasu R, Kumagai Y, Kogetsu H, *et al*. Physiologically based pharmacokinetic model for pralmorelin hydrochloride in rats. Drug Metab Dispos 2005;33:1488–1494.
156. Kiriyama A, Nishiura T, Yamaji H, *et al*. Physiologically based pharmacokinetics of KNI 272, a tripeptide HIV 1 protease inhibitor. Biopharm Drug Dispos 1999;20:199–205.
157. Ploeger B, Mensinga T, Sips A, *et al*. A human physiologically-based model for glycyrrhzic acid, a compound subject to presystemic metabolism and enterohepatic cycling. Pharm Res 2000;17:1516–1525.
158. Parrott N, Jones H, Paquereau N, *et al*. Application of full physiological models for pharmaceutical drug candidate selection and extrapolation of pharmacokinetics to man. Basic Clin Pharm Toxicol 2005;96:193–199.
159. Gordi T, Xie R, Jusko WJ. Semi-mechanistic pharmacokinetic/pharmacodynamic modelling of the antimalarial effect of artemisinin. Br J Clin Pharmacol 2005;60:594–604.

160. Chen K, Teo S, Seng KY. Sensitivity analysis on a physiologically-based pharmacokinetic and pharmacodynamic model for diisopropylfluorophosphate-induced toxicity in mice and rats. Toxicol Mech Methods 2009;19:486–497.
161. Timchalk C, Poet TS. Development of a physiologically based pharmacokinetic and pharmacodynamic model to determine dosimetry and cholinesterase inhibition for a binary mixture of chlorpyrifos and diazinon in the rat. Neurotoxicology 2008;29:428–443.
162. Zhang X, Tsang AM, Okino MS, *et al*. A physiologically based pharmacokinetic/pharmacodynamic model for carbofuran in Sprague-Dawley rats using the exposure-related dose estimating model. Toxicol Sci 2007;100:345–359.
163. Yang RS, el-Masri HA, Thomas RS, *et al*. The application of physiologically based pharmacokinetic/pharmacodynamic (PBPK/PD) modeling for exploring risk assessment approaches of chemical mixtures. Toxicol Lett 1995;79:193–200.
164. el-Masri HA, Thomas RS, Benjamin SA, *et al*. Physiologically based pharmacokinetic/pharmacodynamic modeling of chemical mixtures and possible applications in risk assessment. Toxicology 1995;105:275–282.
165. Barton HA, Clewell HJ 3rd. Evaluating noncancer effects of trichloroethylene: dosimetry, mode of action, and risk assessment. Environ Health Perspect 2000;108:323–334.
166. Poet TS, Kousba AA, Dennison SL, *et al*. Physiologically based pharmacokinetic/pharmacodynamic model for the organophosphorus pesticide diazinon. Neurotoxicology 2004;25:1013–1030.
167. Nong A, Tan YM, Krolski ME, *et al*. Bayesian calibration of a physiologically based pharmacokinetic/pharmacodynamic model of carbaryl cholinesterase inhibition. J Toxicol Environ Health A 2008;71:1363–1381.
168. Doerge DR, Young JF, Chen JJ, *et al*. Using dietary exposure and physiologically based pharmacokinetic/pharmacodynamic modeling in human risk extrapolations for acrylamide toxicity. J Agric Food Chem 2008;56:6031–6038.
169. Young JF, Luecke RH, Doerge DR. Physiologically based pharmacokinetic/pharmacodynamic model for acrylamide and its metabolites in mice, rats, and humans. Chem Res Toxicol 2007;20:388–399.
170. Brochot A, Zamacona M, Stockis A. Physiologically based pharmacokinetic/pharmacodynamic animal-to-man prediction of therapeutic dose in a model of epilepsy. Basic Clin Pharmacol Toxicol 2010;106:256–262.
171. Gerlowski LE, Jain RK. Physiologically based pharmacokinetic modeling: principles and applications. J Pharm Sci 1983;72:1103–1127.
172. Verwei M, van Burgsteden JA, Krul CA, *et al*. Prediction of *in vivo* embryotoxic effect levels with a combination of *in vitro* studies and PBPK modelling. Toxicol Lett 2006; 165:79–87.
173. Chiu WA, Okino MS, Evans MV. Characterizing uncertainty and population variability in the toxicokinetics of trichloroethylene and metabolites in mice, rats, and humans using an updated database, physiologically based pharmacokinetic (PBPK) model, and Bayesian approach. Toxicol Appl Pharmacol 2009;241:36–60.
174. Ernstgard L, Andersen M, Dekant W, *et al*. Experimental exposure to 1,1,1,3,3-pentafluoropropane (HFC-245fa): uptake and disposition in humans. Toxicol Sci 2010; 113:326–336.
175. Gentry PR, Covington TR, Mann S, *et al*. Physiologically based pharmacokinetic modeling of arsenic in the mouse. J Toxicol Environ Health A 2004;67:43–71.
176. Matthews JL, Schultz I, Easterling MR, *et al*. Physiologically based pharmacokinetic modeling of dibromoacetic acid in F344 rats. Toxicol Appl Pharmacol 2010;244:196–207.
177. Gustafson DL, Thamm DH. Pharmacokinetic modeling of doxorubicin pharmacokinetics in dogs deficient in abcb1 drug transporters. J Vet Intern Med 2010;24:579–586.
178. Campbell A. Development of PBPK model of molinate and molinate sulfoxide in rats and humans. Regul Toxicol Pharmacol 2009;53:195–204.

179. Lohitnavy M, Lu Y, Lohitnavy O, *et al*. A possible role of multidrug resistance-associated protein 2 (Mrp2) in hepatic excretion of PCB126, an environmental contaminant: PBPK/PD modeling. Toxicol Sci 2008;104:27–39.
180. Sweeney LM, Kirman CR, Gargas ML, *et al*. Contribution of trichloroacetic acid to liver tumors observed in perchloroethylene (perc)-exposed mice. Toxicology 2009;260:77–83.
181. Evans MV, Chiu WA, Okino MS, *et al*. Development of an updated PBPK model for trichloroethylene and metabolites in mice, and its application to discern the role of oxidative metabolism in TCE-induced hepatomegaly. Toxicol Appl Pharmacol 2009;236:329–340.
182. Young JF, Branham WS, Sheehan DM, *et al*. Physiological "constants" for PBPK models for pregnancy. J Toxicol Environ Health 1997;52:385–401.
183. Ginsberg G, Hattis D, Russ A, *et al*. Physiologically based pharmacokinetic (PBPK) modeling of caffeine and theophylline in neonates and adults: implications for assessing children's risks from environmental agents. J Toxicol Environ Health A 2004;67:297–329.
184. McMahon TF, Medinsky MA, Birnbaum LS. Age-related changes in benzene disposition in male C57BL/6 N mice described by a physiologically based pharmacokinetic model. Toxicol Lett 1994;74:241–253.
185. Timchalk C, Kousba A, Poet TS. Monte Carlo analysis of the human chlorpyrifos-oxonase (PON1) polymorphism using a physiologically based pharmacokinetic and pharmacodynamic (PBPK/PD) model. Toxicol Lett 2002;135:51–59.
186. Johnson TN, Boussery K, Rowland-Yeo K, *et al*. A semi-mechanistic model to predict the effects of liver cirrhosis on drug clearance. Clin Pharmacokinet 2010;49:189–206.
187. Zhang Y, Zhang L, Abraham1 S, *et al*. Assessment of the impact of renal impairment on systemic exposure of new molecular entities: evaluation of recent new drug applications. Clin Pharmacol Ther 2009;85:305–311.
188. Dani M, Boisvert C, Michaud J, *et al*. Short communication. Down-regulation of liver drug-metabolizing enzymes in a murine model of chronic renal failure. Drug Metab Dispos 2010;38:357–360.
189. Wojtal KA, Eloranta JJ, Hruz P, *et al*. Changes in mRNA expression levels of solute carrier transporters in inflammatory bowel disease patients. Drug Metab Dispos 2009;37:1871–1877.
190. Lee C-M, Pohl J, Morgan ET. Dual mechanisms of CYP3A protein regulation by proinflammatory cytokine stimulation in primary hepatocyte cultures. Drug Metab Dispos 2009;37:865–872.
191. Schmith VD, Foss JF. Inflammation: planning for a source of pharmacokinetic/pharmacodynamic variability in translational studies. Clin Pharmacol Ther 2010;87: 488–491.
192. Edginton AN, Theil FP, Schmitt W, *et al*. Whole body physiologically-based pharmacokinetic models: their use in clinical drug development. Expert Opin Drug Metab Toxicol 2008;4:1143–1152.
193. Yoshikawa T, Sugiyama Y, Sawada Y, *et al*. Effect of pregnancy on tissue distribution of salicylate in rats. Drug Metab Dispos 1984;12:500–505.
194. Olanoff LS, Anderson JM. Controlled release of tetracycline—III: A physiological pharmacokinetic model of the pregnant rat. J Pharmacokinet Biopharm 1980;8:599–620.
195. Gabrielsson JL, Paalzow LK. A physiological pharmacokinetic model for morphine disposition in the pregnant rat. J Pharmacokinet Biopharm 1983;11:147–163.
196. Gabrielsson JL, Paalzow LK, Nordstrom L. A physiologically based pharmacokinetic model for theophylline disposition in the pregnant and nonpregnant rat. J Pharmacokinet Biopharm 1984;12:149–165.
197. Gabrielsson JL, Johansson P, Bondesson U, *et al*. Analysis of methadone disposition in the pregnant rat by means of a physiological flow model. J Pharmacokinet Biopharm 1985;13:355–372.

198. Gabrielsson JL, Johansson P, Bondesson U, *et al*. Analysis of pethidine disposition in the pregnant rat by means of a physiological flow model. J Pharmacokinet Biopharm 1986;14:381–395.
199. Bjorkman S. Prediction of drug disposition in infants and children by means of physiologically based pharmacokinetic (PBPK) modelling: theophylline and midazolam as model drugs. Br J Clin Pharmacol 2005;59:691–704.
200. Edginton AN, Schmitt W, Willmann S. Development and evaluation of a generic physiologically based pharmacokinetic model for children. Clin Pharmacokinet 2006;45:1013–1034.
201. Johnson TN, Rostami-Hodjegan A, Tucker GT. Prediction of the clearance of eleven drugs and associated variability in neonates, infants and children. Clin Pharmacokinet 2006;45:931–956.
202. Thompson CM, Johns DO, Sonawane B, *et al*. Database for physiologically based pharmacokinetic (PBPK) modeling: physiological data for healthy and health-impaired elderly. J Toxicol Environ Health B Crit Rev 2009;12:1–24.
203. Inoue S, Howgate EM, Rowland-Yeo K, *et al*. Prediction of *in vivo* drug clearance from *in vitro* data. II: potential inter-ethnic differences. Xenobiotica 2006;36:499–513.
204. Dickinson GL, Lennard MS, Tucker GT, *et al*. The use of mechanistic DM-PK-PD modelling to assess the power of pharmacogenetic studies-CYP2C9 and warfarin as an example. Br J Clin Pharmacol 2007;64:14–26.
205. Rowland M, Matin SB. Kinetics of drug-drug interactions. J Pharmacokinet Biopharm 1973;1:553–567.
206. Ito K, Iwatsubo T, Kanamitsu S, *et al*. Prediction of pharmacokinetic alterations caused by drug-drug interactions: metabolic interaction in the liver. Pharmacol Rev 1998;50:387–412.
207. Brown HS, Ito K, Galetin A, *et al*. Prediction of *in vivo* drug-drug interactions from *in vitro* data: impact of incorporating parallel pathways of drug elimination and inhibitor absorption rate constant. Br J Clin Pharmacol 2005;60:508–518.
208. Obach RS, Walsky RL, Venkatakrishnan K. Mechanism-based inactivation of human cytochrome p450 enzymes and the prediction of drug–drug interactions. Drug Metab Dispos 2007;35:246–255.
209. Venkatakrishnan K, Obach RS. Drug-drug interactions via mechanism-based cytochrome P450 inactivation: points to consider for risk assessment from *in vitro* data and clinical pharmacologic evaluation. Curr Drug Metab 2007;8:449–462.
210. Ripp SL, Mills JB, Fahmi OA, *et al*. Use of immortalized human hepatocytes to predict the magnitude of clinical drug-drug interactions caused by CYP3A4 induction. Drug Metab Dispos 2006;34:1742–1748.
211. Kanamitsu S, Ito K, Sugiyama Y. Quantitative prediction of *in vivo* drug-drug interactions from *in vitro* data based on physiological pharmacokinetics: use of maximum unbound concentration of inhibitor at the inlet to the liver. Pharm Res 2000;17:336–343.
212. Kang HJK, Wientjes MG, Au JLS. Physiologically based pharmacokinetic models of 2,3-dideoxyinosine. Pharm Res 1997;14:337–344.
213. Kato M, Shitara Y, Sato H, *et al*. The quantitative prediction of CYP-mediated drug interaction by physiologically based pharmacokinetic modeling. Pharm Res 2008; 25:1891–1901.
214. Perdaems N, Blasco H, Vinson C, *et al*. Predictions of metabolic drug-drug interactions using physiologically based modelling: Two cytochrome P450 3A4 substrates coadministered with ketoconazole or verapamil. Clin Pharmacokinet 2010;49:239–258.
215. Lin JH, Sugiyama Y, Hanano M, *et al*. Effect of product inhibition on elimination kinetics of ethoxybenzamide in rabbits. Analysis by physiological pharmacokinetic model. Drug Metab Dispos 1984;12:253–256.
216. Quinney SK, Zhang X, Lucksiri A, *et al*. Physiologically based pharmacokinetic model of mechanism-based inhibition of CYP3A by clarithromycin. Drug Metab Dispos 2010;38:241.

217. Shibata N, Gao W, Okamoto H, *et al*. Drug interactions between HIV protease inhibitors based on physiologically-based pharmacokinetic model. J Pharm Sci 2002;91:680–689.
218. Luecke RH, Wosilait WD. Drug elimination interactions: analysis using a mathematical model. J Pharmacokinet Biopharm 1979;7:629–641.
219. Zhang X, Quinney SK, Gorski J, *et al*. Semiphysiologically based pharmacokinetic models for the inhibition of midazolam clearance by diltiazem and its major metabolite. Drug Metab Dispos 2009;37:1587–1597.
220. Shitara Y, Nagamatsu Y, Wada S, *et al*. Long-lasting inhibition of the transporter-mediated hepatic uptake of sulfobromophthalein by cyclosporin A in rats. Drug Metab Dispos 2009;37:1172–1178.